Aus der Klinik für Strahlentherapie
der Medizinischen Fakultät Charité – Universitätsmedizin Berlin

DISSERTATION

Regelschleife für die Magnetresonanz-kontrollierte Teilkörper-Hyperthermie

zur Erlangung des akademischen Grades
Doctor rerum medicarum (Dr. rer. medic.)

vorgelegt der Medizinischen Fakultät
Charité – Universitätsmedizin Berlin

von

Mirko Weihrauch

aus Bochum

Gutachter: 1. Prof. Dr. med. P. Wust

2. Prof. Dr. L. Schad

3. Prof. Dr. rer. nat. J. Beuthan

Datum der Promotion: 14. Juni 2009

Meiner Frau Sonja
und meinen Kindern
Émile, Janko und Maja

Inhaltsverzeichnis

Publikationsliste

Die Publikationen sind nach dem Erscheinungsdatum sortiert.

[1] Gellermann J., M. Weihrauch, C. H. Cho, W. Wlodarczyk, H. Fähling, R. Felix, V. Budach, M. Weiser, J. Nadobny und P. Wust: *Comparison of MR-thermography and planning calculations in phantoms.* Med. Phys., 33(10):3912–3920, Oct 2006.

Impact Factor: 3.571

[2] Gellermann J., J. Göke, R. Figiel, M. Weihrauch, C. H. Cho, V. Budach, R. Felix und P. Wust: *Simulation of different applicator positions for treatment of a presacral tumour.* Int J Hyperthermia, 23(1):37–47, Feb 2007.

Impact Factor: 1.866

[3] Weihrauch M., P. Wust, M. Weiser, J. Nadobny, S. Eisenhardt, V. Budach und J. Gellermann: *Adaptation of antenna profiles for control of MR guided hyperthermia (HT) in a hybrid MR-HT system.* Med. Phys., 34(12):4717–4725, Dec 2007.

Impact Factor: 3.571

Abstract

Seit einigen Jahren werden bei der Hyperthermietherapie mit Radiofrequenzen (RF-Hyperthermie) moderne, MR-gängige Multiantennen-Applikatoren eingesetzt, die eine gezielte Steuerung der Leistungsdichte (SAR: spezifische Absorptionsrate) und ein Monitoring der Temperaturverteilung im Patienten während der Therapie ermöglichen (MR-Thermometrie, z. B. durch Ausnutzung der PRFS: proton resonance frequency shift). Die Steuerparameter für die Ansteuerung der Applikatoren werden durch Hyperthermie-Planungsrechnungen (FDTD: finite-difference time-domain, FE: finite element) vor der Therapie ermittelt. Ziel dieser Arbeit war die Hyperthermieplanung während der Therapie auf Basis der MR-Thermometriedaten so anzupassen, dass eine verbesserte Ansteuerung berechnet werden kann (Regelung).

Die in dieser Arbeit vorgestellten Studien wurden an einem MR-HT-Hybridsystem (1,5 T Magneton Symphony, Siemens, in Verbindung mit dem Sigma-Eye-Applikator des BSD 2000/3D-Systems) mit der Planungssoftware AmiraHyperplan durchgeführt.

In allen Studien konnte die prinzipielle Übereinstimmung der Therapieplanung auf Grundlage von Planungsrechnungen erstmals in 3D belegt werden. Asymmetrien im Abstrahlverhalten des Hyperthermieapplikators (Sigma-Eye) waren nicht nachweisbar. Der visuelle Vergleich zeigte im heterogenen Phantom teilweise jedoch qualitative Abweichungen zwischen Vorhersage und Messung [1]. In Simulation von unterschiedlichen Applikatorpositionen bei der Behandlung eines schwierig zu erwärmenden präsakralen Tumors [2] konnte demonstriert werden, dass eine klinisch wirksame Temperatur ($> 40°C$) im angestrebten Zielgebiet (Tumor) unabhängig von der Applikatorposition erst mit optimierten Steuerparametern erreicht werden kann. Die speziell auf die jeweilige Gewebegeometrie optimierten Steuerparameter erwiesen sich zudem als empfindlicher gegenüber Positionierungsfehlern verglichen mit den „bewährten Standardeinstellungen“.

Die Lösung eines nichtlinearen Ausgleichsproblems für die Antennenprofile (ausgestrahlten elektrischen Felder der einzelnen Antennen) durch die Minimierung der Abweichung von gemessener zu aus den Antennenprofilen berechneter SAR ermöglichte, nach jeder MR-Thermometriemessung die Antennenprofile zu adaptieren. Die Adaptation ist besonders effizient bei Verwendung eines physikalisch sinnvollen Modells als Startwert für die Antennenprofile (Planungsrechnungen, z. B. FDTD). In Weihrauch et. al. [3] konnte an Phantomen demonstriert werden, dass bereits nach einer MR-Thermometriemessung im Mittel eine Verbesserung der Therapievorhersage um 40% im Vergleich zur Standardplanung (FDTD) möglich ist. Nach Vorliegen von zwei MR-Thermometriemessungen konnte die Vorhersagegenauigkeit gegenüber der Standardplanung sogar verdoppelt werden.

Das hier vorgestellte Verfahren ermöglicht eine gezielte Ansteuerung des Hyperthermieapplikators durch die deutliche Verbesserung der SAR-Vorhersage nach bereits einer MR-Thermometriemessung. Hierdurch wird eine Etablierung dieser Regelung der Magnetresonanz-kontrollierten Teilkörper-Hyperthermie im klinischen Einsatz möglich.

1 Einleitung

An der Charité wurde ein MR-HT-Hybridsystem durch Integration eines Sigma-Eye Applikators in einem 1,5T MR Scanner etabliert [4]. Dieses Hybridsystem ermöglicht nichtinvasiv Messungen von 3D-Temperaturverteilungen innerhalb von Phantomen und Patienten auf Basis von MR-Daten [1, 5–7]. Der Sigma-Eye Applikator gewährleistet mit seinen 12 Kanälen (24 Antennen) eine gute Steuerbarkeit bei effektiven Temperaturverteilungen [8–11].

Die Therapieplanung erfolgt auf Grundlage von Planungsrechnungen, der FDTD (finite-difference time-domain [12–14]) oder der FE (finite element [9, 11, 15]) Methode. Diese Berechnungen haben eine relativ hohe Genauigkeit bei akzeptabler Rechenzeit erreicht (45 *min* auf AMD Prozessor mit 2. 2 GHz) [1, 16–18]. Schwankungen im Verstärker und Kopplungen im Antennennetzwerk führen jedoch zu Phasenfehlern. Notwendige Wartungsarbeiten am Applikator führen durch Änderung der Kontaktwiderstände an Steckverbindungen zu schwer quantifizierbaren Abweichungen des Applikatorverhaltens. Noch unvermeidlicher sind Modellierungsfehler bezüglich Patienten- oder Phantomgeometrie und der Gewebezuordnung (Segmentierung), beziehungsweise der exakten Reproduktion der Positionierung des Patienten oder des Phantoms [1, 2].

Die Hauptaufgabe bei der Therapieplanung ist die individuelle Applikatoransteuerung, bestehend aus Amplitude und Phasenverzögerung für jeden Kanal (Antennenpaar), die für den einzelnen Patienten zu einer optimalen Temperaturverteilung führt.

Es wurden bereits einige Modelle entwickelt [19–25], die unter Ausnutzung eines rückgekoppelten Regelkreises theoretisch eine schrittweise Optimierung der Applikatoransteuerung während einer Messreihe ermöglichen sollen. Aus verschiedenen Gründen sind diese Modelle für den Aufbau einer Regelung am MR-HT-Hybridsystem der Charité nicht geeignet (siehe *Kap. I: Introduction* in Weihrauch et. al. [3] zur detaillierten Diskussion).

2 Zielstellung

Das Ziel der in dieser Arbeit vorgestellten Studien war die Erhöhung der klinischen Wirksamkeit einer Hyperthermiebehandlung durch die Maximierung der Temperatur in dem zu erwärmenden Zielgebiet (Tumor).

Daher sollte zuerst in einer Qualitätskontrolle der (Hyperthermie-)Applikator auf eventuelle Fehlfunktionen und Asymmetrien in der Leistungsabstrahlung untersucht werden. Des Weiteren sollte die Vorhersagegenauigkeit der Leistungsdichteverteilung durch die Planungsrechnungen detailliert analysiert werden

Die zweite Studie sollte klären, ob die Positionierung des Applikators bezüglich des Patienten, bei für die Erwärmung mit dem Sigma-Eye-Applikator schwer zugänglichen Tumoren, einen Einfluss auf die zu erwartende Erwärmung dieser Region hat.

Unter Berücksichtigung der Erkenntnisse aus den beiden Studien sollte ein Verfahren zur Anpassung (Adaptation) der Planungsfelder (Antennenprofile) der regionalen

Hyperthermie auf Basis von MR-Thermometriemessungen entwickelt, in einer Studie an Phantomen verifiziert und die Verbesserung dokumentiert werden.

3 Methodik

In allen Studien wurden Erwärmungsexperimente oder Therapien mit einem Hyperthermieapplikator innerhalb eines Magnetresonanztomographen (MR-HT-Hybridsystem) durchgeführt oder analysiert. Daher wird der Versuchsaufbau an dem MR-HT-Hybridsystem in Kap 3.1 kurz vorgestellt.

Anschließend wird die in den einzelnen Studien verwendete Methodik in den Kap. 3.2 -3.4 erläutert.

3.1 Versuchsaufbau

Das MR-HT-Hybridsystem, mit dem die Erwärmungsexperimente durchgeführt wurden, besteht aus einem MAGNETOM Symphony, 1,5 T von Siemens, in welches der Hyperthermieapplikator (BSD-2000/3D) zentriert positioniert werden kann. Der Hyperthermieapplikator hat 12 separat ansteuerbare Kanäle mit je zwei 16 cm langen Antennen. Durch die Einstellung der Stellparameter (12 Phasendelays und 12 Amplituden) kann die Erwärmungsregion modelliert und aus dem Zentrum des Applikators verschoben werden.

Die Studien [1, 3] wurden an zwei Phantomen, einem homogenen und einem heterogenen durchgeführt. Das heterogene Phantom beinhaltet eine Skelettstruktur im Beckenbereich, welches ähnliche Reflexionen und Hotspots wie an der Knochenstruktur eines Patienten erzeugt.

Die in den Erwärmungsexperimenten oder Therapien erzeugten Temperaturverteilungen wurden durch Ausnutzung der Protonen-Resonanz-Frequenz-Shift aus den Phasendifferenzen zweier MR-Datensätzen berechnet. Die Auswertung der MR-Daten erfolgte an einer separaten Workstation mit der Planungssoftware Amira-HyperPlan. Mit der Entwicklerschnittstelle der Softwareplattform Amira wurden alle für die Studien entwickelten Methoden direkt in die Planungssoftware implementiert.

3.2 Vergleich von MR-Thermometrie und Planungsrechnungen im Phantom (Gellermann et. al. 2006)

Mit der Vergleichsstudie von MR-Thermometrie und Planungsrechnungen im Phantom sollten die Abweichungen zwischen der FDTD-Planung und der tatsächlich detektierten Leistungsdichte (SAR) ermittelt werden. Diese Qualitätskontrolle des Applikators diente auch der Einschätzung, des Bedarfs einer Regelung und der zu erwartenden Verbesserung des Therapieergebnisses durch eine Regelung der MR-gestützten Hyperthermie.

Es wurden je 6 Messreihen mit durchschnittlich 4 unterschiedlichen Erwärmungen am homogenen und am heterogenen Phantom durchgeführt. Durch ein spezielles

Experimentendesign [1] sollte sichergestellt werden, dass aus den resultierenden Erwärmungsverteilungen in guter Näherung die SAR berechnet werden kann.

Als Ausgangsvergleich diente eine Planungsrechnung auf FDTD-Basis mit jeweils zentrierter Positionierung des Phantoms im Applikator im MRT. Die Abweichung zwischen FDTD und Thermometriemessung wurde über den quadratischen Mittelwert der Differenzen für alle Phantomvoxel im Field-of-View (ca. 60 000) für die Standard-Planung ermittelt. Dann wurden mittels einer nachträglichen Optimierung der Stellgrößen durch ein Gradientenverfahren optimiert: zuerst die Phasen bei maximaler Amplitude und dann alle Stellgrößen (Phasen und Amplituden) im Hinblick auf die bestmögliche Übereinstimmung mit der Messung. Anschließend wurden alle drei Vergleiche nochmals mit einer positionskorrigierten Planungsrechnung durchgeführt. Die Positionskorrektur wurde durch eine nachträgliche FDTD-Planungrechnung auf Basis der aus den MR-Daten bestimmten Position des Applikators relativ zum Phantom für jede Messreihe durchgeführt.

3.3 Simulation von unterschiedlichen Applikatorpositionen bei der Behandlung von präsakralen Tumoren (Gellermann et. al. 2007)

Es sollte untersucht werden, ob bei für die Hyperthermie schlecht zugänglichen Tumoren ein Zusammenhang zwischen der Positionierung des Applikators relativ zum Patienten (genauer: zum Tumor) und dem zu erwartenden Behandlungserfolg besteht. Die Simulationen wurden am Modell des heterogenen Phantoms durchgeführt.

Dazu wurde für insgesamt 430 unterschiedliche Applikatorpositionen mit optimierten Stellparametern die Behandlung von präsakralen Tumoren simuliert. Die Simulationen wurden auf Grundlage einer Temperaturvorhersage auf Basis von Antennenprofilen, welche mit der FE-Methode auf Tetraeder-Gittern erstellt wurden, durchgeführt. Lateral (x) wurde die Position um $\pm 4cm$, ventral $\Leftrightarrow$ dorsal (y) um $\pm 5cm$ und caudal $\Leftrightarrow$ cranial (z) um $\pm 10cm$ variiert. Für jede Position wurden durch Minimierung der Zielfunktion (mit T_{ther}=43°C (Tumor) und T_{health}=42°C (maximal zulässige Temperatur im gesunden Gewebe))

$$q = \int_{\substack{C \subset tumor \\ T(x) < T_{ther}}} (T_{ther} - T(x))^2 dx + \int_{\substack{C \not\subset tumor \\ T(x) > T_{health}}} (T(x) - T_{health})^2 dx \qquad (1)$$

die optimale Einstellung der Steuerparameter (je einmal mit und ohne Variation der Amplituden) ermittelt, und je acht die Temperaturverteilung im Hinblick auf das angestrebte Therapieziel beschreibende Parameter errechnet (u. a. T_{90}: erreichte Temperatur in 90% des Tumorvolumens).

Zusätzlich wurden die Abweichungen zwischen angestrebter und tatsächlicher Positionierung bei 20 Patienten rückwirkend untersucht.

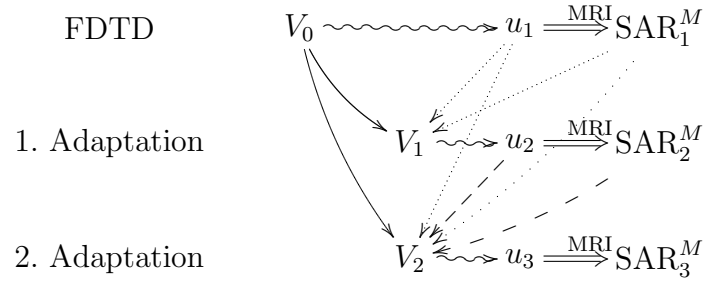

Abbildung 1: Sukzessive Adaptation der Antennenprofile V. Die Steuerparameter u können bestimmt werden durch die Optimierung einer geeigneten Zielfunktion, sobald neue Messungen vorliegen (Regelkreis). MRI bedeutet MR-Thermometriemessung zur Bestimmung der SAR-Verteilung. Die Pfeile beschreiben den Dateninput für jeden Iterationsschritt. Die Doppelpfeile ($\Rightarrow$) repräsentieren die MR-Messungen. Die geschlängelten Pfeile ($\rightsquigarrow$) stehen für die Auswahl oder Optimierung der Steuerparameter u_i

3.4 Adaptation der Antennenprofile zur Regelung der MR-gestützten Hyperthermie (Weihrauch et. al. 2007)

In dieser Arbeit wurde ein Verfahren vorgestellt, welches die elektromagnetischen Antennenprofile V mit Hilfe von MR-Thermometriedaten adaptiert. Ausgehend von der Bio-Heat-Transfer-Gleichung wurde ein nichtlineares Ausgleichsproblem formuliert und mit einem Gauß-Newton-Verfahren gelöst. Dies geschieht durch einen sukzessiven (nach jeder Messung) Abgleich zwischen berechneter SAR und aus der Messung abgeleiteter SAR (SAR_M) (Abb. 1). Durch eine Optimierung der Steuerparameter u nach jedem Identifizierungsschritt, zum Beispiel auf eine ROI (region of interest, z. B. Tumorregion), ließe sich eine Online Regelung der regionalen Hyperthermie aufbauen. Die initialen Startwerte der einzelnen Antennenprofile V wurden durch eine Hyperthermie-Planungsrechnung (FDTD-Methode) ermittelt..

Der experimentelle Messaufbau und die Auswertung der Vorhersagen aufgrund der adaptierten Antennenprofile ist analog zur Studie *Vergleich von MR-Thermometrie und Planungsrechnungen im Phantom (Gellermann et. al. 2006)* [1]. Das Verfahren wurde in 17 Messreihen am Phantom untersucht (4 am homogenen und 13 am heterogenen Phantom).

4 Ergebnisse

4.1 Vergleich von MR-Thermometrie und Planungsrechnungen im Phantom (Gellermann et. al. 2006)

Die Standard-Antennenprofile (FDTD) zeigen im Mittel eine gute Übereinstimmung mit der tatsächlich gemessenen SAR ($\Delta\mathrm{SAR} < 5\ W/kg$). Die nachträgliche Optimie-

rung der Steuerparameter verbessert die Übereinstimmung signifikant um ca. 2 W/kg ($\Delta\mathrm{SAR} < 3\ W/kg$). Die Positionskorrektur führt zu einer weiteren Verbesserung von $0,5\ W/kg$. Im Mittel zeigen die Standard-Antennenprofile im homogenen Phantom eine bessere Übereinstimmung mit den Messungen als im heterogenen. Daher ist die Verbesserung der Übereinstimmung aufgrund der nachträglichen Optimierungen und Positionskorrekturen im heterogenen Phantom größer.

Es gibt Gruppen von Kanälen die unabhängig von den untersuchten Ansteuerungen stärker korrigiert wurden (bezüglich Phase und Amplitude) als andere. Diskrepanzen wurden zwischen allen Kanalgruppierungen detektiert links $\Leftrightarrow$ rechts, oben $\Leftrightarrow$ unten, zentral $\Leftrightarrow$ peripher, lateral $\Leftrightarrow$ vertikal, wobei letztere Gruppe eine fast doppelt so hohe Phasendiskrepanz im Vergleich zu „oben $\Leftrightarrow$ unten“ aufweist.

4.2 Simulation von unterschiedlichen Applikatorpositionen bei der Behandlung von präsakralen Tumoren (Gellermann et. al. 2007)

Die Untersuchung der Positionierungsgenauigkeit an 20 Patienten ergab eine gute Übereinstimmung in x-Richtung ($\pm 1cm$) und y-Richtung ($\pm 2cm$). Am kritischsten erwies sich die z-Richtung (längst der MR-Röhre) mit bis zu $6cm$ Abweichung.

Die mittlere Temperatur im Tumor (T_{90}) bei allen Simulationsrechnungen kann von 38°C bei Standardeinstellungen auf 40°C bei optimierten Steuerparametern erhöht werden. Allerdings nur durch eine deutliche Erhöhung der Applikatorleistung, ermöglicht durch geringere Erwärmung des gesunden Gewebes (Gl. 1, T_{health}) bei optimalen Steuerparametern.

Die Untersuchung der Relation zwischen Applikatorposition und T_{90} im Tumor zeigt bei einer Fehlpositionierung in x-Richtung (links $\Leftrightarrow$ rechts) die geringste Änderung, bei der y-Richtung (ventral $\Leftrightarrow$ dorsal) die größten Änderungen. Bei der z-Richtung (caudal $\Leftrightarrow$ cranial) konnte für die Position z=$8cm$ bei optimierten Steuerparametern die höchste T_{90} erzielt werden. Es konnten noch in anderen Positionen mit geringeren Verschiebungen aus der zentralen Position bessere T_{90}-Werte erzielt werden, als in der zentralen Position.

4.3 Adaptation der Antennenprofile zur Regelung der MR-gestützten Hyperthermie (Weihrauch et. al. 2007)

Die Abweichungen zwischen gemessener und vorhergesagter SAR-Verteilung in Abhängigkeit von der Anzahl der für die Adaptation herangezogenen Messungen k zeigt Tabelle 1. Der relative Fehler ist die Abweichung der Vorhersagen bezüglich der auf eins normierten Abweichung der Standardantennenprofile (FDTD). Die berechnete SAR basierend auf den adaptierten Antennenprofilen ($k > 0$) zeigt eine signifikant bessere Übereinstimmung mit der tatsächlich gemessenen SAR: Im homogenen Phantom konnte die Abweichung um 30% und im heterogenen Phantom sogar um 50% reduziert werden.

	homogenes Phantom			heterogenes Phantom		
k	n	ΔSAR $[W/kg]$	relativer Fehler	n	ΔSAR $[W/kg]$	relativer Fehler
0	20	3.5 ± 0.8	1.0 ± 0.0	64	3.9 ± 0.8	1.0 ± 0.0
1	82	2.8 ± 1.0	0.8 ± 0.2	256	2.3 ± 0.8	0.6 ± 0.2
2	132	2.5 ± 0.9	0.7 ± 0.2	396	2.1 ± 0.7	0.5 ± 0.2
3	104	2.4 ± 0.7	0.7 ± 0.2	292	2.0 ± 0.7	0.5 ± 0.2
4	40	2.4 ± 0.6	0.7 ± 0.1	100	2.1 ± 0.7	0.5 ± 0.2

Tabelle 1: Abweichungen zwischen berechneter und gemessener SAR. k ist die Anzahl der Messungen, die für die Adaptation verwendet wurden. $k = 0$ entspricht dem Startwert (FDTD). n ist die Anzahl der untersuchten Vorhersagen summiert über alle Messreihen.

5 Diskussion

Die Qualitätskontrolle des HT-MR-Hybridsystems beim *Vergleich von MR-Thermometrie und Planungsrechnungen im Phantom* [1] validiert die gute Übereinstimmung zwischen Hyperthermieplanung (FDTD) und Kontrollmessung. Eine Verbesserung der Übereinstimmung um ca. 10% kann durch die nachträglichen Optimierungen erreicht werden. Diese Ergebnisse können jedoch nicht zu einer Anpassung der Planungsrechnungen oder Umbauten am Applikator verwendet werden, da zwar signifikante Unterschiede zwischen dem Phasenkorrekturverhalten einzelner Antennengruppen vorlagen, im Mittel jedoch keine signifikanten Abweichungen einzelner Kanäle nachgewiesen werden konnte.

Die Vergleichsabbildungen ([1], Fig. 2-4) zeigen, dass der berechnete Vergleich der Leistungsdichteverteilung (mind. 50 000 Voxeln) nicht den visuellen ersetzt. Hier sind die Planungsrechnungen mit retrospektiv optimierten Steuerparametern oft besser, als der berechnete Leistungsdichteunterschied vermuten lässt. Die visuelle Darstellung der Therapievorhersagen auf Basis der FDTD zeigt, dass diese häufig nicht die dann tatsächliche gemessene Erwärmungsverteilung im Phantom ausreichend genau widerspiegeln.

Die zweite Studie *Simulation von unterschiedlichen Applikatorpositionen bei der Behandlung von präsakralen Tumoren* [2] unterstreicht durch die Auswertung von 20 Patiententherapien die Notwendigkeit einer geeigneten Regelung der Teilkörperhyperthermie bei schwer zu erwärmenden Tumoren. In allen Richtungen traten Abweichungen von mehreren Zentimetern von der angestrebten Positionierung auf.

Die T_{90} (Temperatur, die in 90% des Zielvolumens erreicht wird) konnte im Mittel um ca. 2°C durch eine Optimierung der Steuerparameter in allen 430 berechneten Positionierungen des Applikators bezüglich des Patienten erhöht werden. Die Berechnungen zeigen auch, dass eine stärkere Erwärmung der Zielregion nur mit höheren Applikatorleistungen, durch Schonung des gesunden Gewebes bei optimalen Einstellungen, erreichbar ist. Allerdings sind diese optimierten Steuerungen empfindlicher gegenüber Phasen und Amplitudenschwankungen. Das bedeutet jedoch auch

im Umkehrschluss, dass eine vorab berechnete Ansteuerung des Applikators durch die zu erwartende Fehlpositionierung während der Therapie nicht den gewünschten Therapieerfolg bringen kann.

Besonders interessant ist die ermittelte Längsverschiebung des Applikators um 8 cm als optimale Positionierung des Patienten, die allerdings ebenfalls zu Kosten einer geringeren Stellparametertoleranz geht.

In der dritten Arbeit [3]: *Adaptation der Antennenprofile zur Regelung der MR-gestützten Hyperthermie* wurde ein Verfahren am Phantom validiert, mit dem eine Anpassung der Planungsfelder unter der Therapie möglich ist.

Der relative Fehler der vorhergesagten Leistungsdichteverteilung in der Tabelle 1 konvergiert bereits nach wenigen Messungen (1-3) gegen einen festen Wert. Beim Phantom ist das ein plausibles Verhalten, da sich „die Physik“ in 1-4 Messungen nicht sonderlich stark oder relativ linear ändert (elektrische Konduktivität). Es gibt im Gegensatz zum Patienten keine Perfusion und keine Bewegungsartefakte in den Themometriedaten zu berücksichtigen. Trotzdem hat die Verbesserung der Vorhersagegenauigkeit der Antennenprofile (Planungsfelder) um 40% in heterogenen Medien nach bereits einer Messung alle Erwartungen übertroffen. Die erste Messung liefert größtenteils schon alle Informationen zur Adaptation der Antennenprofile. Die weiteren Messungen bringen nur noch einen geringen zusätzlichen Informationsgewinn.

Das wichtige Ergebnis dieser Studie ist, dass das entwickelte Verfahren die Antennenprofile nicht nur richtig, sondern auch schnell anpasst. Das ist zum Aufbau einer Regelung der MR-gestützten Hyperthermie essentiell, da hier neben der Eigenbewegung im Körper und der Perfusion, noch die Bewegung des Patienten als feldverändernde Größen in den Thermometriedaten hinzukommen. Daher war diese Studie ein wichtiger Meilenstein auf dem Weg zu einer funktionstüchtigen Regelung der MR-gestützten Hyperthermie. Zusätzlich wird sich die punktweise (voxelweise) Adaptation der vorliegenden Temperaturinformationen vorteilhaft beim Patienten auswirken, da nicht alle Artefakte aus den Thermometriedaten vor der Adaptation entfernt werden müssen. Was beim Patienten vermutlich auch nicht automatisierbar sein wird.

In Weihrauch et. al. [3] konnte am Phantom demonstriert werden, welches Potential eine Regelung der MR-gestützten Hyperthermie hat. Bei einer zusätzlichen Berücksichtigung der Temperaturdiffusion und Perfusion im Patienten, lässt das Verfahren auf eine deutliche Verbesserung der Therapievorhersage nach bereits einer MR-Thermometriemessung hoffen.

5.1 Ausblick

Das vorgestellte Verfahren wird seit einem halben Jahr am Patienten evaluiert. Durch eine optimierte Implementierung der Algorithmen benötigt die Adaptation mit anschließender Optimierung der Stellparameter (Regelung) nur noch 1-2 *sec* Rechenzeit pro berücksichtigte MR-Thermometriemessung ($\approx$ 10 x schneller). Ein verbessertes Adaptationsverfahren mit Berücksichtigung der Temperaturdiffusion und Perfusion in den verschiedenen Geweben wird gerade am Patienten evaluiert.

Veröffentlichungen über die neuen Verfahren und Ergebnisse am Patienten sind in Vorbereitung.

sonstige Literatur

[4] Wust P., J. Gellermann, M. Seebass, H. Fähling, W. Wlodarczyk, J. Nadobny, B. Rau, B. Hildebrandt, A. Oppelt und R. Felix: *Teilkörperhyperthermie mit einem Radiofrequenz-Multiantennen-Applikator unter on-line Kontrolle in einem 1,5 T MR-Tomographen.* Fortschr Röntgenstr, 176:363–374, 2004.

[5] Gellermann J., W. Wlodarczyk, A. Feussner, H. Fähling, J. Nadobny, B. Hildebrandt, R. Felix, and P. Wust: *Methods and potentials of magnetic resonance imaging for monitoring radiofrequency hyperthermia in a hybrid system.* Int. J. Hyperthermia, 21(6):497–513, Sep 2005.

[6] Gellermann J., W. Wlodarczyk, B. Hildebrandt, H. Ganter, A. Nicolau, B. Rau, W. Tilly, H. Fähling, J. Nadobny, R. Felix, and P. Wust: *Noninvasive magnetic resonance thermography of recurrent rectal carcinoma in a 1.5 Tesla hybrid system.* Cancer Res., 65(13):5872–5880, Jul 2005.

[7] Gellermann J., B. Hildebrandt, R. Issels, H. Ganter, W. Wlodarczyk, V. Budach, R. Felix, P.-U. Tunn, P. Reichardt, and P. Wust: *Noninvasive magnetic resonance thermography of soft tissue sarcomas during regional hyperthermia: correlation with response and direct thermometry.* Cancer, 107(6):1373–1382, Sep 2006.

[8] Wust P., M. Seebass, J. Nadobny, P. Deuflhard, G. Mönich, and R. Felix: *Simulation studies promote technological development of radiofrequency phased array hyperthermia.* Int. J. Hyperthermia, 12(4):477–494, 1996.

[9] Paulsen K. D., S. Geimer, J. Tang, and W. E. Boyse: *Optimization of pelvic heating rate distributions with electromagnetic phased arrays.* Int. J. Hyperthermia, 15(3):157–186, 1999.

[10] Kroeze H., J. B. V. de Kamer, A. A. D. Leeuw, and J. J. Lagendijk: *Regional hyperthermia applicator design using FDTD modelling.* Phys. Med. Biol., 46(7):1919–1935, Jul 2001.

[11] Seebass M., R. Beck, J. Gellermann, J. Nadobny, and P. Wust: *Electromagnetic phased arrays for regional hyperthermia: optimal frequency and antenna arrangement.* Int. J. Hyperthermia, 17(4):321–336, 2001.

[12] Yee K. S.: *Numerical solution of initial boundary value problems involving Maxwell's equitations in isotropic media.* IEEE Trans. Antennas Propagat., 17:585–589, 1966.

[13] Sullivan D. M., O. P. Gandhi, and A. Taflove: *Use of the finite-difference time-domain method for calculating EM absorption in man models.* IEEE Trans. Biomed. Eng., 35(3):179–186, Mar 1988.

[14] Taflove A.: *Computational Electrodynamics. TheFinite-Difference Time-Domain Method.* Artech House, Boston, London, 1995.

[15] Beck R., P. Deuflhard, R. Hiptmair, R. H. W. Hoppe, and B. Wohlmuth: *Adaptive multilevel methods for edge element discretizations of Maxwell's equations.* Surv. Math. Ind., 8:271–312, 1999.

[16] Nadobny J., H. Fähling, M. J. Hagmann, P. F. Turner, W. Wlodarczyk, J. M. Gellermann, P. Deuflhard, and P. Wust: *Experimental and numerical investigation of feed-point parameters in a 3-D hyperthermia applicator using different FDTD models of feed networks.* IEEE Trans. Biomed. Eng., 49(11):1348–1359, Nov 2002.

[17] Gellermann J., W. Wlodarczyk, H. Ganter, J. Nadobny, H. Fähling, M. Seebass, R. Felix, and P. Wust: *A practical approach to thermography in a hyperthermia/magnetic resonance hybrid system: validation in a heterogeneous phantom.* Int. J. Radiat. Oncol. Biol. Phys., 61(1):267–277, Jan 2005.

[18] Nadobny J., W. Wlodarczyk, L. Westhoff, J. Gellermann, R. Felix, and P. Wust: *A clinical water-coated antenna applicator for MR-controlled deep-body hyperthermia: a comparison of calculated and measured 3-D temperature data sets.* IEEE Trans. Biomed. Eng., 52(3):505–519, Mar 2005.

[19] Hutchinson E., M. Dahleh, and K. Hynynen: *The feasibility of MRI feedback control for intracavitary phased array hyperthermia treatments.* Int. J. Hyperthermia, 14(1):39–56, 1998.

[20] Arora D., M. Skliar, and R. B. Roemer: *Model-predictive control of hyperthermia treatments.* IEEE Trans. Biomed. Eng., 49(7):629–639, Jul 2002.

[21] Kowalski M. E., B. Behnia, A. G. Webb, and J.-M. Jin: *Optimization of electromagnetic phased-arrays for hyperthermia via magnetic resonance temperature estimation.* IEEE Trans. Biomed. Eng., 49(11):1229–1241, Nov 2002.

[22] Kowalski M. E. and J. M. Jin: *A temperature-based feedback control system for electromagnetic phased-array hyperthermia: theory and simulation.* Phys. Med. Biol., 48(5):633–651, Mar 2003.

[23] Das S. K., E. A. Jones, and T. V. Samulski: *A method of MRI-based thermal modelling for a RF phased array.* Int. J. Hyperthermia, 17(6):465–482, 2001.

[24] Köhler T., P. Maass, P. Wust, and M. Seebass: *A fast algorithm to find optimal controls of multiantenna applicators in regional hyperthermia.* Phys. Med. Biol., 46(9):2503–2514, Sep 2001.

[25] Cheng K.-S., V. Stakhursky, P. Stauffer, M. Dewhirst, and S. Das: *Online feedback focusing algorithm for hyperthermia cancer treatment.* Int. J. Hyperthermia, 23(7):539 – 554, Oct 2007.

Comparison of MR-thermography and planning calculations in phantoms

J. Gellermann
Radiological Unit, Charité Universitätsmedizin Berlin, Campus Berlin Buch, Lindenberger Weg 80, 13125 Berlin, Germany

M. Weihrauch, C. H. Cho, and W. Wlodarczyk
Clinic for Radiation Medicine, Charité Universitätsmedizin Berlin, Campus Virchow Klinikum, Augustenburger Platz 1, 13353 Berlin, Germany

H. Fähling
Radiological Unit, Charité Universitätsmedizin Berlin, Campus Berlin Buch, Lindenberger Weg 80, 13125 Berlin, Germany

R. Felix
Clinic for Radiation Medicine, Charité Universitätsmedizin Berlin, Campus Virchow Klinikum, Augustenburger Platz 1, 13353 Berlin, Germany

V. Budach
Clinic for Radiotherapy, Charité Universitätsmedizin Berlin, Campus Charité Mitte, Schumannstrasse 20-21, 10098 Berlin, Germany

M. Weiser
Konrad-Zuse-Zentrum, Department Numerical Analysis and Modeling, Takustr. 7, 14195 Berlin, Germany

J. Nadobny and P. Wust[a)]
Clinic for Radiation Medicine, Charité Universitätsmedizin Berlin, Campus Virchow Klinikum, Augustenburger Platz 1, 13353 Berlin, Germany

(Received 3 February 2006; revised 28 June 2006; accepted for publication 26 July 2006)

A systematic comparison of three-dimensional MR (magnetic resonance) thermography and planning calculations in phantoms for the hyperthermia (HT) SIGMA-Eye applicator. We performed 2×6 experiments in a homogeneous cylindrical and a heterogeneous elliptical phantom by adjusting 82 different patterns with different phase control inside an MR tomograph (Siemens Magnetom Symphony, 1.5 Tesla). For MR thermography, we employed the proton resonance frequency shift method with a drift correction based on silicon tubes. For the planning calculations, we used the finite-difference time-domain (FDTD) method and, in addition, modeled the antennas and the transforming network. We generated regions according to a segmentation of bones and tissue, and used an interpolation technique with a subgrid of 0.5 cm size at the interfaces. A Gauss-Newton solver has been developed to adapt phases and amplitudes. A qualitative agreement between the planning program and measurements was obtained, including a correct prediction of hot spot locations. The final deviation between planning and measurement is in the range of 2–3 W/kg, i.e., below 10%. Additional HT phase and amplitude adaptation, as well as position correction of the phantom in the SIGMA-Eye, further improve the results. HT phase corrections in the range of 30–40° and HT amplitude corrections of ±20–30% are required for the best agreement. The deviation |MR-FDTD|, and the HT phase/amplitude corrections depend on the type of phantom, certain channel groups, pattern steering, and the positioning error. Appropriate agreement between three-dimensional specific absorption rate distributions measured by MR-thermography and planning calculations is achieved, if the correct position and adapted feed point parameters are considered. As long as feed-point parameters are uncertain (i.e., cannot be directly measured during therapy), a prospective planning will remain difficult. However, we can use the information of MR thermography to better predict the patterns in the future even without the knowledge of feed-point parameters. [DOI: 10.1118/1.2348761]

Key words: hyperthermia planning, magnetic resonance thermography, annular-phased array, phantom

I. INTRODUCTION

One of the methods widely used for solving the Maxwell's equations for hyperthermia (HT) problems is the finite-difference time-domain (FDTD) method.[1] For many years, the FDTD method has been used for HT treatment planning.[2–5] There are HT-specific problems with the FDTD, such as the inclusion of the antennas[6] or transforming networks[7] into the models. These issues are still under investigation. In addition, the precise calculation of the E-fields at (arbitrarily sloped) electrical boundaries is difficult, because in general—their geometry does not fit in the cubical FDTD

lattice. As correctives, various FDTD subgridding and/or subcellular techniques have been developed.[2,8–12] First a postprocessing FDTD corrector for sloped interfaces,[2] or a FDTD field-zooming-technique[11] have been added to the HT-treatment planning software. Wust *et al.*[13] showed that this FDTD corrector[2] improves the accuracy for E-field calculations in inhomogeneous region-based patient models, choosing the volume-surface integral-equation (VSIE) method as reference.[14]

A validation of planning systems, which is based on these numerical methods, is difficult for a real clinical situation. Clearly, the numerical methods can be tested by code comparisons and, in particular, comparison with analytical test cases.[2,6,12] However, the real situation of a heat treatment is much more complicated: and therefore, measurement methods are needed which can be compared with the planning calculations.

One approach attempts to correlate clinical data with planning calculations, either extracted from *in vivo* measurements [e.g., specific absorption rates (SAR)] or clinical observations (e.g., location and intensity of hot spots). This has been successfully performed by Gellermann *et al.*[15] and Sreenivasa *et al.*[16] Limited by the clinical setting, these tests are incomplete and qualitative.

More data are gained with phantom setups. Here, SAR distributions in homogeneous phantoms have been measured by using a variety of methods, such as single E-field sensors,[17,18] scanning devices with E-field sensors,[19,20] lamp matrices,[21] and Schottky diode sheets.[22] For these easy test cases with homogeneous phantoms, often under laboratory conditions, agreement between measurements and planning calculations can be achieved. However, even under these experimental conditions, no systematic comparison of complete three-dimensional (3D) datasets with calculations, i.e., 3D SAR distributions in a phantom, has been performed. In particular, systematic comparisons of patterns in *inhomogeneous* phantoms and calculations are missing.

Recently, magnetic resonance (MR) thermography has been introduced during clinical heat treatments by integration of a HT applicator into the MR bore.[23,24] This enables acquisition of 3D MR-temperature datasets (and SAR datasets) in homogeneous and heterogeneous phantoms.[25,26] The acquisition of these MR-temperature datasets is much faster than in any method before (achieved in some minutes), and, in addition, provides a 3D dataset in 50,000–100,000 grid points. Therefore, comparisons of these datasets with corresponding calculations are more significant. Also, Nadobny *et al.*[27] performed a comparison of MR measured and calculated 3D temperature datasets in an inhomogeneous phantom for an experimental applicator in a limited number of 16 probe position points.

In the following, we present a systematic comparison of a large number of MR-temperature measurements with planning calculations for the SIGMA-Eye applicator (operating HT frequency=100 MHz). Special care is devoted to a classification of the deviations between measurements and plans. In particular, a new Gauss-Newton solver is described for adapting measured and calculated HT phases and amplitudes.

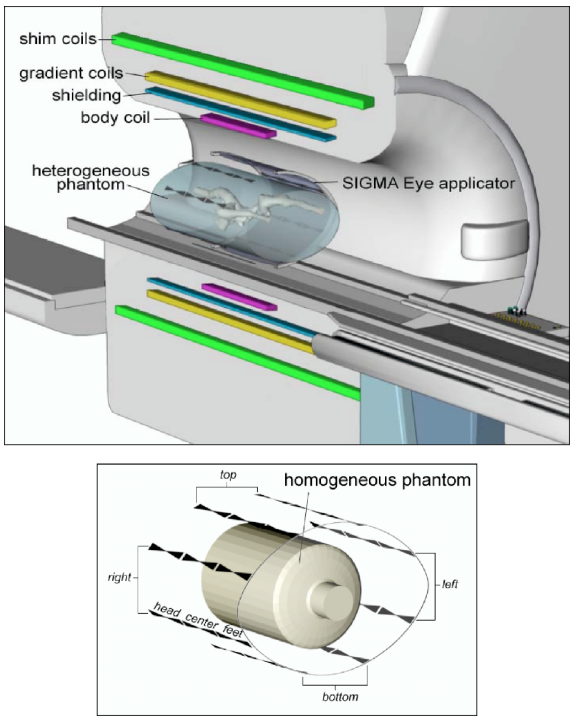

FIG. 1. Experimental setup. The positioning of the SIGMA-Eye applicator and both phantoms in the MR system is shown schematically. Note the indications of three applicator rings (head, center, and feet) and four applicator quadrants (right, left, top, and bottom). The applicator has 12 power channels, each channel connected via transforming networks to two dipoles.

II. MATERIAL AND METHODS

A. Experimental setup

We accomplished our heating experiments in two phantoms, centered in the SIGMA-Eye applicator, which was positioned in the MR bore according to Fig. 1. The Phantom 1 has the shape of a circular cylinder with 30 cm diameter and 40 cm length. It is homogeneously filled with a so-called "superstuff" (σ=0.55 S/m, ε_r=78, equivalent to the so-called "two-thirds medium"). The Phantom 2 has the shape of an elliptical cylinder of $21\times35\times50$ cm, with a skeleton embedded into a tissuelike agarose (two-thirds medium, see above). For further details, see Gellermann.[23]

The MR-compatible SIGMA-Eye HT applicator (BSD Corp., Salt Lake City, Utah) has dimensions of $40\times58\times50$ cm. It can be inserted into the bore of a 1.5 T MR tomograph (Magnetom Symphony, Siemens, Erlangen, Germany) using a special rail system. Technical details describing an operation of the HT applicator under simultaneous MR monitoring have been presented previously.[23,25] The power deposition patterns in the phantoms can be controlled by adjusting the (forward) HT phases and the powers of the 12 channels of the HT applicator. For a detailed description of the SIGMA-Eye applicator (especially in terms of modeling its feed networks) and experimental and numerical inves-

tigation of the relationship between its forward and feed point parameters (HT amplitudes and phases), see Nadobny.[7] Details of modeling, measurements and, proposed improvements can also be found in Wust *et al.*[20,28]

The temperature (increment) distributions that are generated in the phantoms during the heating intervals were acquired three-dimensionally by means of MR-thermography. A summary of available methods is outlined by Gellermann *et al.*[26] Our experiments were based on the proton resonance frequency shift method,[29] which had been shown to provide the most accurate information about temperatures. In all experiments, we used a spoiled echo gradient sequence with TR=750 ms and two echo times TE=4 ms and 20 ms, and flip angle=50°. 40 slices (1 cm slice thickness without gap), with a matrix size of 128×128 and a field of view (FOV) of 50 cm, were acquired. The total acquisition time was 2 min.

We measured a reference MR phase distribution before power-on, and calculated the temperature increments after a heating interval utilizing a calibration factor of 0.01 ppm/°C.

We extracted the temperature information from the MR phase difference between two echo times (double-echo method). This method corrects for temperature-dependent propagation effects (caused by temperature dependencies of the electrical constants). The latter is the reason for relevant temperature errors in homogeneous phantoms filled with large amounts of media with electrical conductivity σ.[26]

Another phenomenon disturbing the MR phase is the local drift of the static magnetic field B0, which is corrected by a special drift correction. For this, we utilized four silicon oil tubes positioned at the bottom right, bottom left, top right, and top left boundaries of the HT applicator. No significant temperature-dependent MR phase shift occurs in silicon oil, and therefore, referring to these regions, we can correct those MR phase changes that are not caused by the temperature increase. A similar correction had been successfully applied under clinical conditions (the so-called fat correction).[25]

Uncorrected MR phase datasets were acquired with the user software of the MR scanner (Siemens SYNGO software platform). These datasets were postprocessed in a planning station using the platform AMIRA-HyperPlan in order to calculate and to visualize the drift-corrected MR-temperature (increment) distributions.[16] These methods were recently validated[23,27] with a temperature accuracy of better than 0.5 °C. We efficiently checked this accuracy using four temperature probes placed in catheters and comparing these direct measurements with MR temperatures.

In particular, during a heating experiment, we verified the linear dependence of the temperature increase over time by direct temperature measurements. However, this is only ensured as long as the spatial temperature gradients are moderate, i.e., far enough from thermal boundaries where conduction or convection effects play a larger role and this linearity can be lost. Assuming the above linearity, the temperature increment $\Delta T(x,y,z)$ during a heating time Δt can be accurately translated into the SAR by the simple formula:

$$\mathrm{SAR[W/kg]} \approx 67 \times \Delta T(^\circ\mathrm{C})/\Delta t(\mathrm{min}). \quad (1)$$

Further details are found in the literature.[30,31]

A 3D SAR dataset of the matrix $128\times128\times40$ (voxel size $0.4\times0.4\times1$ cm) was registered in the tissue-equivalent portion of the two phantoms. No measurable MR signal was received in the skeletal part of the heterogeneous phantom.

B. Design of the experiments

We performed 2×6 heating experiments with a homogeneous and a heterogeneous phantom. The phantoms were inserted into the HT applicator, and both the phantom and the applicator were carefully centered inside the MR gantry. A slight inevitable deviation from the ideal position was corrected by postprocessing (see below). During each experiment, we applied a variety of HT phase setups, a total number of 38 for the homogeneous phantom, and 44 for the heterogeneous phantom. The 12 HT power channels were, for every experiment, supplied with equal power, 75 W per channel (summing up to a total power of 900 W).

For each single HT phase setup, first, an acquisition of a reference dataset during power-off was performed. Then, we applied 900 W during a 5 min heating interval. Finally, still maintaining the power, an actual MR dataset was acquired, employing an acquisition time of 2 min. After power-off, a waiting time of 5 min was selected until acquisition of the next reference dataset.

A time interval of 5 min was estimated as sufficient to achieve a quasi-stationary situation over the whole phantom, and especially around circumscribed regions with formerly high thermal gradients. These critical locations (e.g., at bone surfaces in the heterogeneous phantom), with an extension of a few centimeters, might be exposed to a high SAR and have thermal equilibration times of a few minutes. Clearly, this is not implying that the thermal equilibration of the total volume of >30 kg, which needs several hours. We verified the quasi-steady state by tracking temperature time curves with bowman thermistors in the catheters (see e.g., Ref. 26); requesting a negligible temperature decrease per minute during power-off (<0.02 °C/min), in comparison to the gradient after power-on (of >0.2 °C/min, i.e., >10 W/kg). In addition, we excluded critical domains from the evaluation volume (total matrix on which the deviation between calculation and measurement is accumulated) by specifying a small margin (1 cm) around bone surfaces and shifting the outer boundary of the phantom away from the water bolus. Thus, after a waiting time of 5 min a reasonably well-defined reference MR measurement (still during power-off) can be achieved as the basis for the next SAR distribution. Nevertheless, one should keep in mind the slight intrinsic smoothing effect of our measurement method.

This procedure is repeated several times. We employed either slight pattern shifts (with HT phases ≤10°) or greater displacements (with HT phase delays of 45–90°, corresponding to geometrical pattern shifts up to 5–7 cm). The required HT phases to shift the pattern in a given direction by a certain distance had been previously estimated by elementary geometric considerations,[21,32] and had also been demonstrated in a lamp phantom.[33]

For every pattern, the (forward) HT phases in the channels can be described as a relationship to the so-called "balanced" or "standard" setting. For this setting, a SAR maximum in the center of the (homogeneous) phantom is generated (verified, e.g., by a lamp phantom). This initial condition can be achieved by adding a phase delay of 40° to the balanced feeding cables of the top and bottom channel (Fig. 1). These delays cause a constructive interference of all channels in the center of the applicator (see also a detailed description of the SIGMA Eye applicator).[7] Amplitudes in every channel remain equal. In addition, an off-set HT phase correction is required for all 12 channels, which compensates for all other influences that unbalance the SAR interference maximum. The achievement of the balanced setting was always a starting point before each experiment.

C. Planning the SAR distributions

The SAR distributions were calculated using the FDTD method on voxel grids of $1\times1\times1$ cm, which were generated from 3D computer tomography datasets of each of the phantoms. This cubical grid is extended to cover the complete SIGMA-Eye applicator and the water bolus, resulting in a regular cubic grid of $80\times80\times80$ cells. For obtaining the SAR, the E-field distributions for every channel (12 complex vector fields) were computed, and then coherently superposed. Calculation time on a standard personal computer is about 10 min per channel. Open boundary conditions were simulated by using the perfectly matched layer formulation according to Berenger[34] and Sullivan.[35] A special interpolation technique on a subgrid of $0.5\times0.5\times0.5$ cm was employed to calculate the E-fields near electrical boundaries.[2]

For obtaining the segmented region-based model, we manually specified the boundaries of the skeleton (and the outer contour automatically), while addressing $\sigma=0.55$ S/m, $\varepsilon_r=78$, to the tissuelike medium (agarose in the real phantom) and $\sigma=0$, $\varepsilon_r=2.8$ to the skeleton (plasticlike bone structures in the real phantom). Such a region-based FDTD approach can be applied in conjunction with the interpolation method at electrical boundaries (2). There was slight tendency to smooth the SAR maxima, but in general a fair agreement has been shown for the region-based FDTD by Wust *et al.*[13] in comparison with competitive methods, which provide particularly accurate results at electrical boundaries, such as the VSIE method.[6,14] The dipole antennas of the SIGMA-Eye applicator and the transforming networks from the coaxial feeding cable to the antenna pair (basically Y-shaped transmission networks with shunt-inductive tuning stubs) were modeled using a combined 3D/one-dimensional (1D) FDTD formulation according to Nadobny *et al.*[7] Employing the FDTD algorithm, and including the transforming networks and antennas into the model, models can predict HT-phase offsets in the feed points, at least via E-field coupling. But, as the 1D modeling of the networks is somewhat idealized, assuming, e.g., a perfect applicator and network symmetry, partly unexplained variations/deviations remain for real networks that cannot be predicted by the present algorithm, as is further outlined in Wust *et al.*[28] and Nadobny *et al.*[7] The 3D/1D FDTD algorithm needs to be further improved for a more precise description of the individual real (to some extent, asymmetric) network behavior.

We started our calculations for both phantoms in a centered standard (balanced) setting as described at the end of Sec. II B (called the *standard model*). In the next step, we corrected for a slight displacement of the phantom in the water bolus (relative to the applicator wall). In a real situation, this displacement cannot be completely prevented, but it can be quantified from the (morphological) T1-weighted dataset of the phantom in the applicator during MR thermography. Following this quantification, a (numerical) transformation of the phantom from the standard position to the imaged position can be performed by matching suitable reference points defined in a phantom. We identified the coordinates of the displacement in the lateral (x), vertical (y), and longitudinal directions (z). The absolute displacement distance Δr can be calculated according to $\Delta r=(\Delta x^2+\Delta y^2+\Delta z^2)^{1/2}$. After appropriate shifting of the phantom, we generated a new regular grid, which described the actual geometry. This new corrected model is called the *position-corrected model*. Planning calculations were performed for every experiment—first for the standard model, and second for the position-corrected model.

D. Comparison of measurements and calculations

In the first step, in order to enable a meaningful comparison, both datasets (MR-temperature, calculated SAR) were appropriately transformed. First, the SAR subgrid, which was given by the FDTD subgrid of $0.5\times0.5\times0.5$ cm, was resampled and positioned in order to match the MR data with a cubic grid of $0.4\times0.4\times1$ cm. We determined the measured $\mathrm{SAR_{MR}}$ according to Eq. (1) on the MR grid, and transformed the calculated SAR to the MR grid ($\mathrm{SAR_{FDTDtrans}}$) by interpolation from the surrounding grid points $k(j)$ ($j=1$–8) of the FDTD-grid ($\mathrm{SAR_{FDTD}}$, at a maximum at eight grid points), according to the following equation (k indexing all grid points):

$$\mathrm{SAR_{FDTDtrans}}(k)=\Sigma_{k(j)}(1-|\mathbf{r_{kMR}}-\mathbf{r_{jFDTD}}|)/R*\mathrm{SAR_{jFDTD}},$$
$$\mathbf{R}=\Sigma_{\mathbf{k(j)},j=1-8}\,(1-|\mathbf{r_{kMR}}-\mathbf{r_{jFDTD}}|). \quad (2)$$

The comparison is performed only on "reliable" grid points, i.e., grid points in agarose (two-thirds medium) located at least 1 cm from the outer phantom boundary. Each point of the skeleton, either in the MR measurement or from the SAR calculation was edited from comparison, because all skeletal grid points give no evaluable MR signal. This "safety margin" around the electrical boundaries was necessary because we used two different echo times (TE=4 ms and 20 ms) for MR thermography, which result in slightly different spatial information during the reconstruction process (MR-frequency and -phase encoding). As a consequence, the double-echo method (subtraction of MR phases at different echo times) entails uncertainties in regions with large MR

phase gradients, i.e., especially near boundaries.

Furthermore, we restricted our comparison to 20 central slices (distance between slices was 1 cm), i.e., to a 20 cm long central part of the FOV (MR), because of the highest homogeneity of the MR B0 fields and thus highest accuracy of the MR acquisition in this zone. In addition, we identified all MR-grid points with unusually large signal differences to the surrounding voxels, and replaced them by the mean value calculated from the surrounding grid points. This was necessary because of unavoidable inhomogeneities of the agarose material in the phantom (e.g., small air regions around catheter tunnels for temperature probes and the catheters themselves). We refer to the points belonging to this reduced phantom part, that were used for the comparison, as "selected points".

Moreover, we scaled the measured and calculated data by equalizing the cumulative total power for both (MR and FDTD) data sets under comparison. This resulted in a replacement of SAR_{FDTD} by $c*SAR_{FDTD}$, with the following scaling factor c:

$$c = \Sigma_{j=1-N} SAR_{jMR} / \Sigma_{j=1\ldots N} SAR_{jFDTD}, \quad (3)$$

where N is the number of selected grid points.

We quantified the difference between the theoretical plan (FDTD data set) and the MR measurement (MR data set) by the quadratic mean of the differences of the SAR in W/kg:

$$|MR - FDTD| = (\Sigma_{j=1-N}(SAR_{jMR} - SAR_{jFDTD})^2/N)^{1/2}, \quad (4)$$

where N is the number of selected grid points.

The number of reliable grid points available for the comparison was $N > 50{,}000$.

We applied three methods to determine |MR-FDTD| and to improve the agreement, step by step:

- Step 1 (assigning the selected control parameters): HT (forward) phases were selected at the terminal of the HT-treatment system and the additional offsets were considered. All forward HT amplitudes (powers) at the channels were set equal to 75 W/channel during each experiment.
- Step 2 (phase adaptation): HT phases were varied during the superposition of FDTD E-fields (total of 12 E-fields, each for 1 HT channel) until the mean quadratic difference [Eq. (4)] achieved a local minimum. The HT phases used in Step 1 were specified as the starting values.
- Step 3 (phase and amplitude adaptation): HT phases obtained in Step 2 were used as a starting phase set, but this time a variation of both HT phases and HT amplitudes was allowed in order to minimize |MR -FDTD| [Eq. (4)].

For searching a local minimum of |MR-FDTD|, we employed a solver–based on a gradient method—and stopped the searching process if the difference of subsequent |MR -FDTD| deviation sets fell below 1%, i.e., around some 0.001 W/kg. This was typically achieved after 30–50 iteration steps.

Finally, we systematically determined the |MR-FDTD|, as well as the HT phase corrections $\Delta\Phi_j$ and corrected powers P_j, dependent on the phantoms, the models (standard and position corrected), the searching methods (Steps 1–3), and the selected patterns (central or peripheral). The dependencies were validated statistically by the Wilcoxon test for linked and the Mann-Whitney test for unconnected samples.

The search for both HT phases and amplitudes around the selected control parameters, as performed in Methods 2 and 3, is not only justified, but even required because phase shifts and amplitude differences of these parameters occur in the antenna of the real SIGMA-Eye applicator.[7,20,28] A crucial problem was identified in the measurement and correction of feed point parameters in multiantenna applicators. The complex feed point voltages are especially important because they are directly related to the main component (z) of the E-field-interference pattern (and therefore, SAR) inside the applicator, although the pattern characteristics are more influenced by changing the antenna phases.

III. Results

In general, we have found a qualitatively good agreement between the measured (MR) and calculated (FDTD) patterns ($\Delta SAR < 5$ W/kg) with increasing congruence, either by going from Method 1 to Methods (steps) 2 or 3 ($\Delta SAR < 3$ W/kg), and/or by replacing the standard model (centered position) by the model based on the corrected position of the phantom (decrease of ΔSAR by 0.5 W/kg). In Fig. 2, the best agreement is shown for the position-corrected model after a variation of HT phases and amplitudes. We note that the SAR maxima at electrical boundaries ("hot spots") are very sensitive to the exact position of the boundaries (bone surfaces). Therefore, position-corrected models evidently give a better description of location, extension and size of these hot spots.

However, the agreement is not always as perfect as is illustrated in Fig. 3, where some qualitative differences remain between measurement and theoretical description. The sensitivity on geometrical details is so high that the used model (using a subgrid of 0.5 cm) is not accurate enough to describe the features. Slight imperfections in the description can alter the existence, location, and form of hot spots. Figure 3 illustrates the critical dependence of hot spot formation and, in particular, the improvement by correcting the position.

It had been discussed previously that a tetrahedral grid might be more adequate to describe the geometry of electrical boundaries.[2,21] We did not insist on generating tetrahedral grids because our measured datasets were given on a regular grid, and it was easier to compare the measured data with data of another regular grid (generated for the FDTD method). Our examples demonstrate that the FDTD method, using a subgrid for interpolation at electrical boundaries, is sufficient to predict the SAR distribution, even in inhomogeneous media. Another reason as to why the use of a tetrahedral grid would not improve the results of this comparison is the fact that the MR cannot be measured directly at the

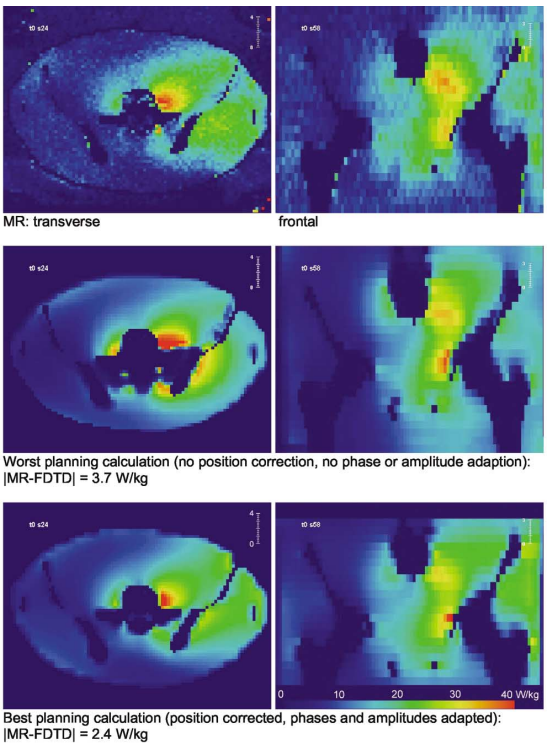

FIG. 2. Comparison of MR thermography with planning for a pattern shifted with 90° to the left. Maximum 50 W/kg. The SAR data set is transformed/resampled with respect to the MR data sets.

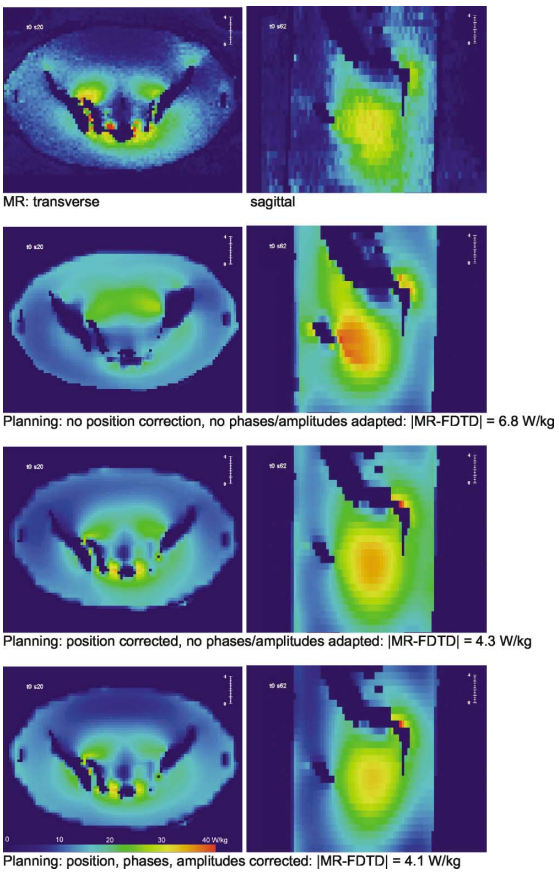

FIG. 3. Comparison of MR thermography with planning for a pattern slightly (14°) shifted to the left and feet. Maximum 56 W/kg. The SAR data set are transformed/resampled with respect to the MR data sets.

boundaries (see Sec. II A). Thus, tetrahedral nodes lying directly at these boundaries would be excluded. As a consequence, a disproportionate high precision at electrical boundaries for the theoretical approach, as is given by the use of the tetrahedral grids, appears unnecessary for this comparison.

We note that the SAR values in the inhomogeneous phantom are 55 W/kg at maximum and 30 W/kg in the homogeneous phantom (see Figs. 2 and 3). The mean deviations |MR-FDTD| range between 2 and 3 W/kg for the more elaborate methods, i.e., better than 10%. This accuracy corresponds to the measurement error, and is satisfactory.[23]

An impressive improvement of |MR-FDTD|, by nearly a factor of 2, is achieved by changing from Method (Step) 1 to Method 2 (with $p<0.0005$) after searching for the correct HT phases in the antenna feed points. There is an additional and still significant ($p<0.05$) improvement, if HT amplitude variations are added. Using the inhomogeneous phantom, the mean deviations |MR-FDTD| are significantly better for the position-corrected model ($p<0.0005$). This again emphasizes the importance of describing the correct position of the phantom (or the patient) in the SIGMA-Eye applicator. An uncorrected position cannot be fully compensated for by the HT phase and amplitude variation when using the inhomogeneous phantom. Interestingly, in case of the homogeneous phantom, a position error can be compensated for by a HT phase adaptation.

|MR-FDTD| are generally smaller using the homogeneous phantom, at least if the feed point parameters are adapted. This again confirms the challenge for calculating the E-fields correctly at electrical boundaries. In the inhomogeneous phantom, the difference between measured and calculated data can be high, even after correcting the position.

The HT phase corrections $\Delta\Phi_i$, are found after the application of Methods 2 and 3. For different experiments (on different days), the phase correction vector can dramatically vary; while during a single experiment from adjustment to adjustment, only moderate additional shifts have been found. There is no significant difference between the two phantoms. However, clear distinctions are found between certain channel groups, probably indicating certain asymmetries of the system and/or the setups. This discrepant behavior is observed between the right and left, top and bottom, central and outer rings, and in particular, if all lateral channels (see Fig. 1) are compared with all vertical channels. Here, the $\Delta\Phi$s are

nearly twice as large for the top/bottom channels. The HT phase corrections, $\Delta\Phi$, are decreased ($p<0.001$), if an appropriate position correction is performed before the search run.

We verified a further (but less significant) decrease of |MR-FDTD|, if the HT amplitudes are adapted together with the HT phases (Method 3). The corrected power values p_i differ no more than 20 and 30 W from the initial values of 75 W per channel, i.e., typically $<30\%$. We note that this is explained by the technical uncertainty of ±15% per channel. Sometimes, the modifications are virtually negligible and grouped near around the initial value of 75 W.

Nevertheless, we identified—similarly to the $\Delta\Phi$—significant differences between channel groups after the search run for Method 3, again reflecting asymmetries. However, a systematic behavior is not discernable. The HT phase corrections are largest, when changing from fixed selected HT phases (Method 1) to a variation of the HT phases alone (Method 2). Here, the mean HT phase corrections amount to $>40°$. The HT phase corrections decrease (around 35°), if HT phases and amplitudes are adapted concurrently (Method 3). Comparing Methods 2 and 3, a small difference of approximately 15° for $\Delta\Phi$ is found. Nevertheless, the range of the HT phase corrections remains between 30–45°.

The HT amplitude correction (Method 3) shows a different behavior when comparing the standard model with the position-corrected model for the two phantoms. While the HT amplitude correction decreases for the heterogeneous phantom (similarly to the HT phase correction), an increase is detected in case of the homogeneous phantom. This phenomenon might be explained by a higher feedback and reflection of the phantom walls when a homogeneous phantom is positioned off-center.[28]

The position errors (corrected by the displacements Δx, Δy, and Δz) were inspected separately. We found a systematic vertical shift between 0.8 to 5.6 cm, caused by the gradual changing of phantom position during the filling of the bolus with water and the lack of correct repositioning. The shift to the side Δx was small (below ±1 cm). The longitudinal shift Δz ranged between −2 and 3.5 cm. We investigated the deviation |MR-FDTD|, dependent on the distance r, for the positioning correction and found no significant difference (using Method 1). The HT phase corrections (calculated by Methods 2 and 3) are even larger for small corrections (<5 cm). This is consistent with the rule that the HT phase errors (induced by various kinds of coupling) increase near the central pattern (balanced or equal-phased adjustment).

We also examined the dependence on the magnitude of pattern steering (below 10° or 45°–90°). In case of the heterogeneous phantom, slight pattern shifts, i.e., central patterns, are associated with the largest HT phase errors. Especially near the equal-phased adjustments, small changes ($<10°$ steering, <5 cm displacement) can induce large disturbances, in particular due to complicated 3D structures. Therefore, these dependencies are not found in the homogeneous phantom.

IV. Discussion

In this study we measured SAR distributions in a homogeneous and a heterogeneous phantom in $>50{,}000$ grid points in a range of 20–60 W/kg, and compared these voluminous experimental data with FDTD calculations. Under the best conditions (adapting HT phases and amplitudes, correcting the position of the phantom), we achieved an agreement of 2–3 W/kg, i.e., an accuracy of better than 10%. This error is in the range of the uncertainty of the measurement itself, which is known as better than 0.5 MR-degrees in the temperature range of 5–15 MR degrees. We achieved consistent results for several consecutive experiments on different days (total of 12 experiments) with different phantoms and a sizeable number of HT phase adaptations.

These highly welcomed results not only validate our planning system in use, but also show, in addition, that MR thermography in phantoms might be useful for quality assurance. Because of this unique data pool, we could elucidate important characteristics of present technology, in particular, concerning multiantenna arrays.

First, the sensitivity of the E-field patterns, in regard to details of the electrical boundaries, has been pointed out in previous publications[21] and has been strikingly confirmed. We could qualitatively describe the 3D SAR distributions in a heterogeneous phantom, including a number or SAR maxima (hot spots) at the bone surface (Figs. 2 and 3). As expected, it is necessary to readjust the position of the phantom, especially if heterogeneities are in the interior of the lossy medium. Even if the HT phases are readapted, this cannot fully replace the correct positioning of the phantom.

Because hot spots are sensitive to details of the boundaries, some differences in the plan may persist (e.g., Fig. 3). It appears, that the measurements show hot spots—to some extent more pronounced in some of the tests than those predicted by the FDTD calculations (as described in Sec. II C). This is noteworthy due to the following reasons. First, our measurement method has the tendency to intrinsically smear out maxima at electrical boundaries. Second, the spatial inaccuracies are a result of subtraction of MR phases belonging to different echo times. Third large thermal conduction occurs in high thermal gradients. On the other hand, our FDTD algorithm, with a regular subgrid of 0.5 cm size, is less accurate directly at the boundaries than algorithms based on tetrahedral grids. This numerical approach is, however, sufficiently accurate under the circumstances of these experiments, because no exact MR data acquisition is possible for points directly located at agarose/bone boundaries. Thus, the accuracy at electrical boundaries has been estimated as good enough for our comparisons. A basic approach to correct even these remaining differences will be outlined below.

Second, even if there is a sophisticated control in the amplifier itself, the HT phases and amplitudes selected in a multiamplifier system can nevertheless severely deviate from the HT phases and amplitudes, which are impressed in the feed points of the antennas.[36] Because the patterns are explicitly dependent on these feed point parameters, we have to correct for the real HT phases. The reasons, mainly originat-

ing from the antenna crosstalking, and the characteristics of these variations have been discussed elsewhere.[7,28] We cannot eliminate these effects because the efficiency of the applicator and degree of coupling (cross-talking) go hand in hand.

The results of our study confirm that seeking good agreement between measurements and calculations yields modifications of the HT phases (at probably the correct parameters). Wust *et al.*[20] came to a similar conclusion by measuring in the SIGMA-Eye applicator using an electro-optic sensor. Adapting the HT phases and amplitudes provides a satisfactory theoretical description of the sensor measurements.[20]

Based on the present study, we gain a more comprehensive and general idea of the technical situation of multiantenna HT applicators. We identify HT phase displacements of 30°–45° and channels where this is especially pronounced (e.g., the vertical antennas at top and bottom).

The variations of the resulting HT amplitudes (powers) in the feed points lead to an improved description, and we found the required adaptions as high as ±20–30% (Method 3). However, we conclude from our analysis, that a significant improvement of the agreement is already obtained if Step 2 (only phases are adapted) is conducted.

The problem of the feed point control has been discussed in the literature. A specific hardware has been proposed to measure the feed point parameters online.[37,38] For HT applicators of the SIGMA-type (containing antenna networks with transmission line bifurcations and jumps of the characteristic line impedance), coaxial measurements are rather insufficient to characterize the feed point parameters.[7] However, HT phase-sensitive measurements in the feed points of available multiantenna applicators might be highly difficult and costly.

On the other hand, it might be cumbersome or virtually impossible to develop algorithms, describing all electrotechnical details of the applicator and the feeding network in order to predict the precise HT phases in the feed points and the exact location and extension of every single hot spot at each boundary.

Therefore, we presently prefer another interesting approach. We intend to recalculate new base functions for every channel conducting a suitable solver. These improved base functions must incorporate all inaccuracies in comparison to the initial plan—in particular, the HT phase errors and all amplitude deviations. Improved base functions should be constructed in a postprocessing tool, which uses the full information derived from a variety of measurements. This innovative, and also a patients-applicable approach, will be the subject of a following paper.

ACKNOWLEDGEMENTS

This work has been supported by grants from the Deutsche Forschungsgemeinschaft (DFG) (project WU 235/1-1) and the Lieselotte Beutel–Stiftung. The authors gratefully acknowledge this support.

[a]Author to whom correspondence should be addressed. Electronic mail: peter.wust@charite.de

[1]K. S. Yee, "Numerical solution of initial boundary value problems involving Maxwell's equations in isotropic media," IEEE Trans. Antennas Propag. **17**, 585–589 (1966).
[2]J. Nadobny, D. Sullivan, P. Wust, M. Seebass, P. Deuflhard, and R. Felix, "A high-resolution interpolation at arbitrary interfaces for the FDTD method," IEEE Trans. Microwave Theory Tech. **46**, 1759–1766 (1998).
[3]D. Sullivan, "Three-dimensional computer simulation in deep regional hyperthermia using the FDTD method," IEEE Trans. Microwave Theory Tech. **38**, 204–211 (1990).
[4]D. Sullivan, *Electromagnetic Simulation Using the FDTD Method* (IEEE Press, New York, 2000).
[5]J. van de Kamer, A. A. de Leeuw, S. N. Hornsleth, H. Kroeze, A. N. Kotte, and J. J. Lagendijk, "Development of a regional hyperthermia treatment planning systems," Int. J. Hyperthermia **17**, 207–220 (2001).
[6]J. Nadobny, R. Pontalti, D. Sullivan, W. Wlodarczyk, A. Vaccari, P. Deuflhard, and P. Wust, "A thin rod approximation for the improved modeling of bare and insulated cylindrical antennas using the FDTD method," IEEE Trans. Antennas Propag. **51**, **1780–1786** (2003).
[7]J. Nadobny, H. Fähling, M. Hagmann, P. Turner, W. Wlodarczyk, J. Gellermann, P. Deuflhard, and P. Wust, "Experimental and numerical investigations of feed-point parameters in a 3D hyperthermia applicator using different FDTD models of feed networks," IEEE Trans. Biomed. Eng. **49**, 1348–1359 (2002).
[8]T. G. Juergens, A. Taflove, K. Umashankar, and T. G. Moore, "Finite-difference time-domain modeling of curved surfaces," IEEE Trans. Antennas Propag. **40**, 357–366 (1992).
[9]A. Taflove, *Advances in Computational Electrodynamics: The Finite-Difference Time-Domain Method* (Artech House, Boston, MA, 1998).
[10]N. Kaneda, B. Houshmand, and T. Itoh, "FDTD analysis of dielectric resonators with curved surfaces," IEEE Trans. Microwave Theory Tech. **45**, 1645–1649 (1997).
[11]J. B. van de Kamer, A. A. de Leeuw, H. Kroeze, and J. J. Lagendijk, "Quasistatic zooming for regional hyperthermia treatment planning," Phys. Med. Biol. **46**, 1017–1030 (2001).
[12]J. Nadobny, D. Sullivan, W. Wlodarczyk, P. Deuflhard, and P. Wust, "A 3D tensor FDTD-formulation for treatment of sloped interfaces in electrically inhomogeneous media," IEEE Trans. Antennas Propag. **51**, 1760–1770 (2003).
[13]P. Wust, J. Nadobny, M. Seebass, D. Stalling, J. Gellermann, H. C. Hege, P. Deuflhard, and R. Felix, "Influence of patient models and numerical methods on predicted power deposition patterns," Int. J. Hyperthermia **15**, 519–540 (1999).
[14]J. Nadobny, P. Wust, M. Seebass, P. Deuflhard, and R. Felix, "A volume-surface integral equation method for solving Maxwell's equations in electrically inhomogeneous media using tetrahedral grids," IEEE Trans. Microwave Theory Tech. **44**, 543–554 (1996).
[15]J. Gellermann, P. Wust, D. Stalling, M. Seebass, J. Nadobny, R. Beck, J. Beier, H. C. Hege, P. Deuflhard, and R. Felix, "Clinical evaluation and verification of the hyperthermia treatment planning system HyperPlan," Int. J. Radiat. Oncol., Biol., Phys. **47**, 1145–1156 (2000).
[16]G. Sreenivasa, J. Gellermann, B. Rau, J. Nadobny, P. Schlag, P. Deuflhard, R. Felix, and P. Wust, "Clinical application of the hyperthermia treatment planning system HyperPlan—Comparison of algorithms and clinical observables," Int. J. Radiat. Oncol., Biol., Phys. **55**, 407–419 (2003).
[17]K. D. Paulsen and M. P. Ross, "Comparison of numerical calculations with phantom experiments and clinical measurements," Int. J. Hyperthermia **6**, 333–349 (1990).
[18]P. Wust, T. Meier, M. Seebass, H. Fähling, K. Petermann, and R. Felix, "Noninvasive prediction of SAR distributions with an electro-optical E-field sensor," Int. J. Hyperthermia **11**, 295–310 (1995).
[19]P. Wust, J. Berger, H. Fähling, J. Nadobny, J. Gellermann, W. Tilly, B. Rau, K. Petermann, and R. Felix, "Scanning E-field sensor device for on-line control of annular-phased-array system," Int. J. Radiat. Oncol., Biol., Phys. **43**, 927–937 (1999).
[20]P. Wust, R. Beck, J. Berger, H. Fähling, M. Seebass, W. Wlodarczyk, W. Hoffmann, and J. Nadobny, "Electric-field distributions in a phased-array applicator with 12 channels—Measurements and numerical simulation," Med. Phys. **27**, 2565–2579 (2000).
[21]P. Wust, H. Fähling, M. Brünner, J. Nadobny, A. Jordan, and R. Felix, "Visualization and registration of three-dimensional E-field distributions in annular-phased-array applicators," Med. Phys. **26**, 653–659 (1999).
[22]G. C. van Rhoon, D. J. van der Heuvel, A. Amezane, P. J. Rietveld, K.

Volenec, and J. van der Zee, "Characterization of the SAR-distribution of the Sigma-60 applicator for regional hyperthermia using a Schottky diode sheet," Int. J. Hyperthermia **19**, 642–654 (2003).
[23]J. Gellermann, W. Wlodarczyk, H. Ganter, J. Nadobny, H. Fähling, M. Seebass, R. Felix, and P. Wust, "A practical approach to thermography in a hyperthermia/MR hybrid system—Validation in a heterogeneous phantom," Int. J. Radiat. Oncol., Biol., Phys. **61**, 267–277 (2005).
[24]J. Gellermann, B. Hildebrandt, R. Issels, H. Ganter, W. Wlodarczyk, V. Budach, R. Felix, P. U. Tunn, P. Reichardt, and P. Wust, "Non-invasive MR-thermography of soft tissue sarcomas during regional hyperthermia: Correlation with response and direct thermometry," Cancer in press (2006).
[25]J. Gellermann, W. Wlodarczyk, B. Hildebrandt, H. Ganter, W. Tilly, H. Fähling, J. Nadobny, R. Felix, and P. Wust, "Noninvasive magnetic resonance thermography of recurrent rectal carcinoma in a 1.5 Tesla hybrid system," Cancer Res. **65**, 1–9 (2005).
[26]J. Gellermann, W. Wlodarczyk, A. Feussner, H. Fähling, J. Nadobny, B. Hildebrandt, R. Felix, and P. Wust, "Methods and potentials of magnetic resonance imaging for monitoring radiofrequency hyperthermia in a hybrid system," Int. J. Hyperthermia **21**, 497–513 (2005).
[27]J. Nadobny, W. Wlodarczyk, L. Westhoff, J. Gellermann, R. Felix, and P. Wust, "A clinical water-coated antenna applicator for MR-controlled deep-body hyperthermia: A comparison of calculated and measured 3D temperature data sets," IEEE Trans. Biomed. Eng. **52**, 505–519 (2005).
[28]P. Wust, H. Fähling, W. Wlodarczyk, M. Seebass, J. Gellermann, P. Deufhard, and J. Nadobny, "Antenna arrays in the SIGMA-Eye applicator: Interactions and transforming networks," Med. Phys. **28**, 1793–1805 (2001).
[29]J. de Poorter, C. de Wagter, Y. de Deene, C. Thomson, and C. Stahlberg, "Noninvasive MRI thermometry with the proton resonance frequency (PRF) method: *In vivo* results in human muscle," Magn. Reson. Med. **33**, 74–81 (1995).
[30]P. Wust, H. Stahl, J. Löffel, M. Seebass, H. Riess, and R. Felix, "Clinical, physiological, and anatomical determinants for radiofrequency hyperthermia," Int. J. Hyperthermia **11**, 151–167 (1995).
[31]W. Tilly, P. Wust, B. Rau, C. Harder, J. Gellermann, P. Schlag, V. Budach, and R. Felix, "Temperature data and specific absorption rates in pelvic tumors: Predictive factors and correlations," Int. J. Hyperthermia **17**, 172–188 (2001).
[32]P. Wust, H. Fähling, R. Felix, S. Rahman, R. Issels, H. J. Feldmann, G. van Rhoon, and J. van der Zee, "Quality control of the SIGMA applicator using a lamp phantom: A four-center comparison," Int. J. Hyperthermia **11**, 755–767 (1995).
[33]P. Wust, H. Fähling, A. Jordan, J. Nadobny, M. Seebass, and R. Felix, "Development and testing of SAR-visualizing phantoms for quality control in rf hyperthermia," Int. J. Hyperthermia **10**, 127–142 (1994).
[34]J. P. Berenger, "A perfectly matched layer for the absorption of electromagnetic waves," J. Comput. Phys. **114**, 185–200 (1994).
[35]D. M. Sullivan, "An unsplit step 3D PML for use with the FDTD method," IEEE Microw. Guid. Wave Lett. **7**, 1984–1986 (1997).
[36]P. Wust, H. Fähling, T. Helzel, M. Kniephoff, W. Wlodarczyk, G. Mönich, and R. Felix, "Design and test of a new multiamplifier system with phase and amplitude control," Int. J. Hyperthermia **14**, 459–477 (1998).
[37]W. M. Lee, A. Ameziane, A. M. van den Biggelaar, P. J. Rietveld, and G. C. van Rhoon, "Stability and accuracy of power and phase measurements of a VVM system designed for online quality control of the BSD-2000 (-3D) DHT system," Int. J. Hyperthermia **19**, 74–88 (2003).
[38]J. Berger, K. Petermann, H. Fähling, and P. Wust, "Calibrated electro-optic E-field sensors for hyperthermia applications," Phys. Med. Biol. **46**, 399–411 (2001).

Gellermann et. al. 2007

Der „Electronic Reprint“ des Artikel

> Gellermann J., J. Göke, R. Figiel, M. Weihrauch, C. H. Cho, V. Budach, R. Felix und P. Wust: *Simulation of different applicator positions for treatment of apresacral tumour.* Int J Hyperthermia, 23(1):37–47, Feb 2007.
> **DOI**: 10.1080/02656730601121549

auf dem Dokumentenserver der Freien Universität Berlin wurde leider nicht genemigt.

Adaptation of antenna profiles for control of MR guided hyperthermia (HT) in a hybrid MR-HT system

Mirko Weihrauch[a)] and Peter Wust
Clinic for Radiation Oncology, Charité–Universitätsmedizin Berlin, Campus Virchow Klinikum, Augustenburger Platz 1, 13353 Berlin, Germany

Martin Weiser
Department Numerical Analysis and Modeling, Zuse Institute Berlin, Takustrasse 7, 14195 Berlin, Germany

Jacek Nadobny, Steffen Eisenhardt, Volker Budach, and Johanna Gellermann
Clinic for Radiation Oncology, Charité–Universitätsmedizin Berlin, Campus Virchow Klinikum, Augustenburger Platz 1, 13353 Berlin, Germany

(Received 15 May 2007; revised 31 August 2007; accepted for publication 2 October 2007; published 16 November 2007)

A combined numerical-experimental iterative procedure, based on the Gauss-Newton algorithm, has been developed for control of magnetic resonance (MR)-guided hyperthermia (HT) applications in a hybrid MR-HT system BSD 2000 3D-MRI. In this MR-HT system, composed of a 3-D HT applicator Sigma-Eye placed inside a tunnel-type MR tomograph Siemens MAGNETOM Symphony (1.5 T), the temperature rise due to the HT radiation can be measured on-line in three dimensions by use of the proton resonance frequency shift (PRFS) method. The basic idea of our iterative procedure is the improvement of the system's characterization by a step-by-step modification of the theoretical HT antenna profiles (electric fields radiated by single antennas). The adaptation of antenna profiles is efficient if the initial estimates are radiation fields calculated from a good *a priori* electromagnetic model. Throughout the iterative procedure, the calculated antenna fields (FDTD) are step-by-step modified by comparing the calculated and experimental data, the latter obtained using the PRFS method. The procedure has been experimentally tested on homogeneous and inhomogeneous phantoms. It is shown that only few comparison steps are necessary for obtaining a dramatic improvement of the general predictability and quality of the specific absorption rate (SAR) inside the MR-HT hybrid system. © *2007 American Association of Physicists in Medicine*. [DOI: 10.1118/1.2804617]

Key words: hyperthermia, MRI, closed-loop control, antenna profiles, FDTD, Gauss-Newton algorithm

I. INTRODUCTION

Regional hyperthermia, performed with phase steered ring applicators like the Sigma-60 applicator, has been in use for 15–20 years. With this technique different groups worldwide have derived extraordinary clinical results in combined therapies with radiation therapy, chemotherapy, and radiochemotherapy.[1–3] Also, the relationship of higher temperatures with improved clinical results has been shown[4,5] (see also Ref. 6 for an overview).

Earlier, model calculations have displayed that navigation and resulting temperature distributions are improved by better applicator design.[7–10] The overall strategy was to increase the number of antennas, resulting in an improved navigation of the power distribution. Applicators according to this design have been constructed and have been in clinical use for a few years (Sigma-Eye applicator with 12 channels compared to four channels in Sigma-60).

The main task in designing a therapy is to come up with an applicator control consisting of amplitude and phase delay for each antenna that leads to an individually optimal temperature distribution inside the patient. There are two essentially different strategies to accomplish this: (a) using physical and physiological models of the applicator and patient, respectively, to compute the electrical fields, energy absorption, and temperature distribution, followed by an *a priori* optimization of the applicator control, and (b) using a feedback control loop to drive the applicator towards the optimal adjustment during the therapy.

Strategy (a) involves solving the time-harmonic Maxwell's equations by FDTD (finite-difference time-domain[11–13]) or FE (finite element[8,10,14]) methods, as well as the bio-heat-transfer equation.[15] Multiple models and planning systems have been developed in the last decades[16–18] and have been evaluated in phantoms.[19–21] In principle, these computations can be performed with relatively high accuracy in acceptable time (45 min on PC: AMD, 2.2 GHz). For example, a combined electromagnetical-thermal comparison between simulations on 1 cm voxel grids and measured 3-D MR-temperature data sets in patients resulted in an average temperature deviation of 0.45 °C, which corresponds to a relative deviation of around 18%.[20] However, inevitable modeling errors in the phantom/patient geometry and tissue behavior, variations in the feeding network, and inaccurate amplifier behavior often lead to inexact results.

Strategy (b) circumvents the need for a correct physical model by directly controlling the temperature during the therapy. In most cases, one or more temperature measurements are necessary for controlling the temperatures, usually achieved by power changes of one or more channels. Here, the characteristics and stability of the controller, e.g., reaction to disturbances, are important to consider.[22,23]

In the hyperthermia related literature some control loops have already been described. If a linear time dependent model $y(t)=-Ku(t)$ mapping the control settings u to the state variables y is assumed, and a quadratic quality functional $J(y)$ is to be minimized, the controller output satisfies a certain matrix equation (so-called Riccati equation).[24] Due to its increasing computational complexity, this method is limited to low-dimensional systems with few control settings and state variables.

The application of such a feedback controller has been mainly focused on the navigation of ultrasound HT applicators. Hutchinson *et al.*[24] proposed a controller based on an increase of temperature (in n measurements) depending on m power levels (of ultrasound transducers). Arora *et al.*[25] presented a formulation for an optimal control, using the descriptors of thermal dosimetry (T90 and thermal dose) by applying a linear approximation of a highly nonlinear problem. The introduction of thermal dose (which continues to accumulate even after power is turned off) required the development of a model predictive controller. In both cited articles, the control plans were applied only for simulated thermal therapies, examining the influences of measurement errors, noise, and imprecision of the model.

At the Charité, a hybrid MR-HT system integrating a Sigma-Eye applicator and an 1.5 T MR scanner has been established.[26] This hybrid system allows noninvasive MR measurements of 3D temperature distributions inside phantoms and patients,[27] and therefore provides the prerequisites to conduct MR-guided regional hyperthermia in a closed control loop.

A transfer of the aforementioned algorithms to MR-guided HT is impractical due to the high number of spatial temperature measurements (state variables y) to be respected. A different control scheme based on MRI monitoring has been introduced by Kowalski *et al.*[28,29] for hyperthermia and applied to a phantom in a quasi-2D applicator with one antenna ring. Their method is based on the representation of the specific absorption rate (SAR) in the form

$$\mathrm{SAR} = u^H M u, \tag{1}$$

where u is the complex control vector and M is a Hermitian action matrix (see also Refs. 30 and 31). In a setup phase, M is identified from MR measurements of many, sufficiently exciting control vectors. Afterwards, Eq. (1) can be used directly to optimize any SAR-dependent quality functional.

With modern applicators with $n=12$ independent channels, such as the Sigma-Eye applicator, and more so for actual therapy, the approach based on complete identification of M has a severe drawback. For an applicator with n independent channels, M contains n^2 degrees of freedom, such that at least n^2 measurements are required for a full identification. For probably this reason, the simulations in Refs. 28 and 29 were restricted to a six-channel applicator and the phantom experiments limited to only three channels. Note that for the Sigma-Eye applicator 144 measurements would be necessary. In a clinical therapy, the required setup phase would last several hours even before the actual treatment could start. Moreover, the control settings for which the measurements are taken have to span the whole control space (called "sufficiently exciting" by Kowalski *et al.*[28,29]). Applied to actual hyperthermia treatments, this means that the patient would have to endure a lot of clinically suboptimal SAR distributions, probably provoking unfavorable physiological counter-regulations.

We are thus facing the challenge to devise a controller that delivers a near-optimal therapy using much fewer measurements than are necessary to perform a full model identification. We therefore propose a different approach combining strategies (a) and (b) mentioned above. Starting with the available, physically well-founded, though only approximative numerical *a priori* models, we adapt them, taking relatively few measurements into account. Such an adaptation scheme is described in the following section. The experimental results given in Sec. III D suggest that this combination of approaches (a) and (b) is quite promising.

II. METHODS

In this section we describe the control scheme. It differs from Kowalski *et al.*[28] in two aspects: *a priori* knowledge from planning computations is taken into account, and the identification is geared towards the antenna profiles instead of the action matrix. Before such an online control with integrated optimization can be applied to hyperthermia treatment of patients, it is necessary to validate the method at phantoms. This validation is to be investigated in the following.

II.A. Mathematical model

The total electrical field E of a hyperthermia applicator with n antennas can be described by a linear combination of the antenna profiles V^ν, $\nu=1,\ldots,n$, radiated by the single antennas:

$$E = \sum_{\nu=1}^{n} u^\nu V^\nu = Vu, \tag{2}$$

where $u^\nu \in \mathbb{C}$ are the complex control settings associated with the amplifier channels.

From the electric field, the SAR can be computed as

$$\mathrm{SAR} = \frac{\sigma}{2}|E|^2 = \frac{\sigma}{2} u^H V^H V u. \tag{3}$$

The superscript H denotes the complex conjugate transpose. Note that the action matrix can be recovered as $M=V^HV$.

The evolution of the temperature distribution inside an unperfused phantom during hyperthermia is described by the time-dependent bio-heat-transfer equation

$$\mathrm{div}(\kappa \nabla T) + \rho \cdot \mathrm{SAR} = \rho c \frac{\partial T}{\partial t}, \tag{4}$$

where T is temperature (K), t is time (s), SAR is specific absorption rate (W/kg), κ is thermal conductivity (W m^{-1} K^{-1}), ρ is density (kg/m^3), and c is heat capacity (W s kg^{-1} K^{-1}). Neglecting thermal diffusion, which is admissible for small κ or smooth temperature distributions, and small time differences Δt, the SAR can be approximated by SAR^M obtained from temperature measurements T^M as SAR^M:

$$\mathrm{SAR} \approx \mathrm{SAR}^M = c \frac{\Delta T^M}{\Delta t}. \tag{5}$$

For further details see Refs. 32 and 33.

II.B. Procedure to adapt the antenna profiles of a hyperthermia applicator

As mentioned in the Introduction, we assume that the initial antenna profiles V_0 obtained from an *a priori* simulation are a reasonable approximation to the antenna profiles V. Given k measurements to arbitrary control settings u_i, $i = 1, \ldots, k$, either V_0 or $M_0 = V_0^H V_0$ can be adapted to V_k or M_k, respectively, such that the computed values

$$\mathrm{SAR}_i = \frac{\sigma}{2} u_i^H V_k^H V_k u_i = \frac{\sigma}{2} u_i^H M_k u_i \tag{6}$$

match the measured data SAR_i^M as closely as possible. Since V consists of n complex-valued vectorial E fields, the number of real degrees of freedom in V is $n*2*3=6n$ compared to n^2 real degrees of freedom in the complex Hermitian matrix M. Thus we feel that for $n>6$ and $k \ll n^2$, the smaller model based on adaptation of V_0 is more appropriate than adaptation of M_0. We therefore aim at minimizing

$$g(V) = \|F(V)\|^2, \tag{7}$$

with

$$F(V) = \begin{pmatrix} \frac{\sigma}{2} u_1^H V^H V u_1 - c \frac{\Delta T_1}{\Delta t_1} \\ \vdots \\ \frac{\sigma}{2} u_k^H V^H V u_k - c \frac{\Delta T_k}{\Delta t_k} \end{pmatrix}. \tag{8}$$

F represents the mismatch between measurements and model prediction. For solving Eq. (7), the Gauss-Newton method (see, e.g., Ref. 34)

$$\Delta V^j = -F'(V^j)^+ F(V^j),$$

$$V^{j+1} = V^j + \Delta V^j, \quad j = 0, \ldots, \tag{9}$$

is applied, where $F'(V^j)^+$ denotes the pseudoinverse of $F'(V^j)$. The iteration (9) is terminated as soon as $\|\Delta V^{j*}\| \leq \varepsilon$ for some j_*, and we set $V_k = V^{j*}$. In our computations we have chosen $\varepsilon = 10^{-5}$. Note that F is not complex differentiable, such that a realification of F has to be used.

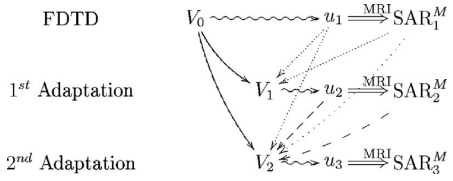

FIG. 1. Successive adaptation of the antenna profiles V. The control settings u can be determined based on the optimization of a quality functional as measurements become available (closed-loop control). MRI denotes the MR measurement for the determination of the SAR. Arrows indicate the input data record for each respective calculation. The double arrow ($\Rightarrow$) stands for the measurement and the sidled arrow ($\rightsquigarrow$) means selection of control settings u_i.

For few measurements, the least squares problem (7) is highly underdetermined, such that infinitely many solutions exist. Since V_0 is assumed to be a physically well-founded approximate solution, it is desirable to choose a solution V_k with minimal distance to V_0. This is realized by application of the pseudoinverse $F'(V^j)^+$ in each Gauss-Newton step. In passing we note that a good initial value V_0 results in a fast local convergence of the Gauss-Newton method.

This leaves the question how to choose the control settings u_i. In principle, any set of sufficiently different control settings can be used for adaptation of the antenna profiles. However, since during actual hyperthermia one will aim at treating the patient with the best therapy currently known, the control settings u_i should rather be computed by optimizing a given quality functional using the best available model V_{i-1}, sequentially as measurements become available (closed-loop control). This procedure is illustrated in Fig. 1.

III. EXPERIMENTS

The practical benefit that can be obtained by adaptation of antenna profiles as described in Sec. II has been evaluated in a series of heating experiments using two different phantoms.

III.A. Experimental setup

The heating experiments were performed in two different phantoms (homogeneous and heterogeneous) centered in the SIGMA-Eye HT applicator (BSD Corp., Salt Lake City, UT) with a size of $40 \times 58 \times 50$ cm^3. The homogeneous phantom has a shape of a circular cylinder of 30 cm diameter and 40 cm length. It is filled with a so-called "superstuff" ($\sigma = 0.55$ S/m, $\epsilon_r = 78$, equivalent to so-called "2/3 medium"). The heterogeneous phantom has a shape of an elliptical cylinder of $21 \times 35 \times 50$ cm^3 with a skeleton embedded into a tissuelike agarose (2/3 medium, see above). For further details see Ref. 19.

The power deposition patterns in the phantoms can be controlled by adjusting the phases and the amplitudes of the 12 channels of the HT applicator. The channel feed antennas are organized in three transversal antenna rings (Feet, Middle, Head). Control settings u_i are specified as phase delays in ventral, dorsal, right, and left channels in each ring.

TABLE I. Workflow of test procedure. Steps 6 and 7 demonstrate the integration of the adaptation procedure in a closed control loop.

	Step	Time (min)	Action
Preparation	I	−51	positioning phantom in the BSD system in the MR scanner
	II	−49	MR measurement
	III	−45	starting calculation of FDTD antenna profiles based on the MR measurement
Measurement cycle 1	1	0	MR thermometry measurement (reference dataset)
	2	2	Power on! 900 W, control setting u_1
	3	7	MR thermometry measurement $\rightarrow \mathrm{SAR}_1^M$
	4	9	Power off!
	5	9	SAR calculation based on the two MR thermometry measurements
In case of online control	6	12	adaptation of antenna profiles
	7	15	optimizing SAR in a target region (closed loop control) → control setting u_2
Measurement cycle 2	1	14 or 17	MR thermometry measurement (reference dataset)
	⋮	⋮	⋮

For a detailed description of the SIGMA-Eye applicator (especially with respect to the modeling of its feed networks) and experimental and numerical investigation of the relationship between its forward and feed point parameters (HT amplitudes and phases), see Ref. 18. Details of modeling, measurements and proposed improvements can also be found in Refs. 35 and 36.

The temperature (increment) distributions that were generated in the phantoms during the heating intervals were acquired three-dimensionally by means of MR thermography. The applicator was inserted into the bore of a 1.5 Tesla MR tomograph (Magnetom Symphony, Siemens, Erlangen, Germany) using a special rail system as described in Ref. 21. Technical details describing an operation of the HT applicator under simultaneous MR monitoring have been presented previously.[19,37]

A summary of available MR thermography methods is outlined in Ref. 27. The experiments were based on the proton resonance frequency shift method (PRFS),[38] which had been shown to provide the most accurate temperature information. In all experiments a spoiled echo gradient sequence with TR=750 ms and two echo times TE=4 and 20 ms, flip angle 50° was used. Forty slices (1 cm slice thickness without gap) with a matrix size of 128×128 and a field of view (FOV) of 50 cm were acquired. The total acquisition time was 2 min.

Uncorrected MR phase datasets were acquired with the user software of the MR scanner (Siemens SYNGO). These datasets were postprocessed in a planning station using AMIRA-HyperPlan[39] in order to calculate and to visualize the drift-corrected MR-temperature (increment) distributions.[36,40] The postprocessing procedure needs about 10 s. These methods were validated[19,20] with a temperature error below 0.5 °C. This accuracy was verified selectively using four temperature probes placed in catheters and comparing these direct measurements with MR temperatures. Further details can be found in Refs. 5 and 21.

A three-dimensional SAR dataset of $128\times128\times40$ voxels of dimensions $0.39\times0.39\times1$ cm^3 each was registered in the tissue-equivalent portion of two phantoms. No measurable MR signal was received in the skeletal part of the heterogeneous phantom.

III.B. Test procedure

The procedure was analyzed in 17 test series. Four of them were performed with the homogeneous phantom, and 13 with the inhomogeneous phantom. First, the initial antenna profiles V_0 were computed using the FDTD method on a Cartesian grid with cells of dimension $1\times1\times1$ cm^3. Special care has been taken to compute the FDTD on the exact geometry given by the actual relative positioning of phantom and HT applicator inside the MR bore. The antenna profiles were then linearly interpolated onto the voxel grid used for obtaining the MR measurements (see formulas A1 and A2 in the Appendix from Ref. 41). Then, during each test series, four different control settings were applied sequentially. For each control setting a reference data set was acquired before heating. After heating with 900 W for $\Delta t=5$ min, the acquisition of another MR dataset (acquisition time $\approx$2 min) starts, with still power on (Table I). Note that Δt must be clearly longer than the temperature acquisition time ($\approx$123 s) during the MR sequence in order to suppress intra-acquisitional smoothing effects. The choice of the particular

TABLE II. Deviations between measured and computed SAR. k is the number of measurements used to adapt the antenna profiles, $k=0$ corresponds to the FDTD. n is the number of predicted measurements, summed up over all test series.

		Homogeneous phantom			Heterogeneous phantom	
k	n	ΔSAR (W/kg)	Relative error	n	ΔSAR (W/kg)	Relative error
0	20	3.5±0.8	1.0±0.0	64	3.9±0.8	1.0±0.0
1	82	2.8±1.0	0.8±0.2	256	2.3±0.8	0.6±0.2
2	132	2.5±0.9	0.7±0.2	396	2.1±0.7	0.5±0.2
3	104	2.4±0.7	0.7±0.2	292	2.0±0.7	0.5±0.2
4	40	2.4±0.6	0.7±0.1	100	2.1±0.7	0.5±0.2

heating time interval $\Delta t \approx 5$ min as used in this paper is explained in Ref. 20 (Sec. IV B 2iii). Furthermore, from our long-term MR-measurement experience, we notice that the applied power of 900 W guarantees an average temperature rise of around 3 °C during the aforementioned heating time interval, which is a value clearly higher than the general MR-measurement accuracy of around 0.5 °C. From the temperature difference of both datasets, a measurement SAR^M is computed according to Eq. (5).

After each SAR measurement, the power was switched off for an appropriate time (≈5 min) until a quasi-stationary state had been reached (see B. Design of the experiments in Ref. 21). For most test series, the next control setting was determined by simultaneously maximizing the SAR in some region of interest and minimizing the SAR outside this region on the base of the adapted antenna profiles (see Fig. 1 and Table I). On the other hand, complementary control settings were adjusted in test series, e.g., 5 cm left, 5 cm right, 5 cm ventral, 5 cm dorsal in the axial plane, because the aim of this investigation is to examine the adaptation procedure. After the equilibration period, the measurement cycle for the next control settings was started (Table I). The duration of one measurement cycle amounts to 14 min. The adaptation of the antenna profiles can be calculated after the whole test procedure, if the control settings were determined before the measurements start (Table I).

III.C. Comparison of measurement and planning

It is important to note that the least-squares approach (7)–(9) is independent of any ordering of the measurements in one test series, even if the control settings were obtained by successive optimization. Moreover, arbitrary subsets of test series can be used in a retrospective analysis for assessing the possible benefit of the presented approach for correctly predicting SAR distributions.

Since Eq. (7) is underdetermined, exact reproduction of SAR distributions for control settings u_i can be expected when the corresponding measurement SAR_i^M is included in the set used for adapting the antenna profiles. This trivial case is, of course, not the aim of our comparison. We are investigating the improvement of predictability. Therefore, in the results presented below, the measurement to which the computed SAR is compared is never included in the set of measurements used to adapt the antenna profiles. An example for a possible comparison: The measured SAR_3^M in the third measurement cycle can be compared with the computed $\mathrm{SAR}_I=(\sigma/2)u_3^H V_0^H V_0 u_3$ based on the standard antenna profiles V_0 and with the computed $\mathrm{SAR}_{II}=(\sigma/2)u_3^H V_2^H V_2 u_3$ based on the adapted antenna profiles V_2, which were adapt from the two measurement cycles before (see Fig. 1 and Table I).

Deviations between measured and computed SAR distributions are quantified by the root mean square error

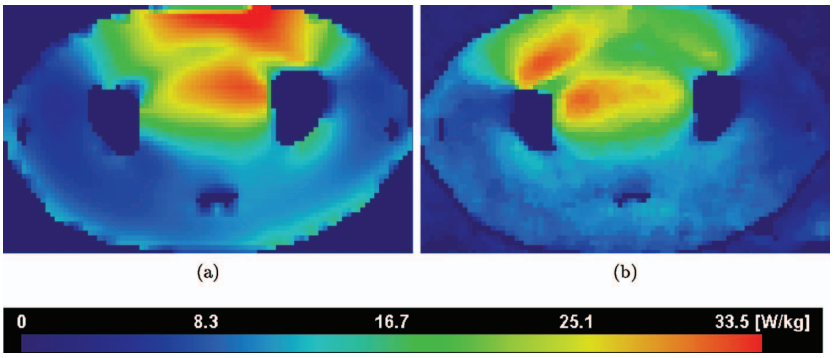

FIG. 2. Comparison of FDTD [(a) $\mathrm{SAR}(V_0,u_a)$] and measurement [(b) $\mathrm{SAR}^M(u_a)$] in a transversal plane for the control setting u_a={Feet (31,114,60,43) Middle (97,59,37,0) Head (56,43,32,44)}. The deviation is ΔSAR=4.7 W/kg. Maximal measured SAR in the 3-D field of view (FOV): 53.2 W/kg, averaged measured SAR in FOV: 14.8 W/kg.

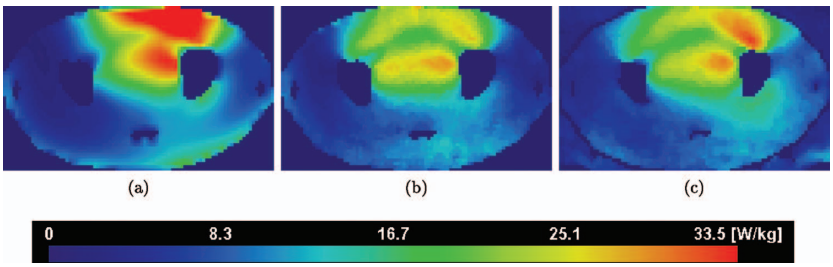

FIG. 3. Improvement of SAR prediction for the control setting u_b={Feet (40,139,82,69) Middle (112,63,0,1) Head (57,45,29,35)} by adaptation of antenna profiles based on only one measurement for a *different* control setting u_a (in Fig. 2). (a) FDTD simulation for u_b: SAR(V_0,u_b), (b) Improved SAR prediction SAR(V_1,u_b), and (c) associated measurement SAR^M(u_b). Notice that (b) depends on the measurement SAR^M(u_a) shown in Fig. 2(b) via the adapted antenna profiles V_1 computed by the Gauss-Newton algorithm. The deviation between (b) and (c) is reduced to ΔSAR=2.6 W/kg compared to the FDTD simulation of SAR(V_0,u_b) in (a) with ΔSAR=4.0 W/kg. Maximal measured SAR in the FOV: 45.8 W/kg, averaged measured SAR in FOV: 14.2 W/kg.

$$\Delta\mathrm{SAR} = \sqrt{\frac{1}{N}\sum_{i=1}^{N}(\mathrm{SAR}^M(v_i) - s\mathrm{SAR}(v_i))^2},$$

where the computed SAR is normalized to yield the same total power as the measured SAR by

$$s = \frac{\sum_{i=1}^{N}\mathrm{SAR}^M(v_i)}{\sum_{i=1}^{N}\mathrm{SAR}(v_i)}.$$

Here, N is the number of voxels v_i for which reliable MR data was available. In particular, voxels in skeletal regions and close to tissue boundaries were excluded from comparison. For all test series, at least 60 000 voxels were used.

The adaptation of the antenna profiles based on the FDTD planning, as described in Fig. 1, lasted around "k minutes" (k: number of measurements) with a PC: P IV, 1.5 GHz.

III.D. Results

Deviations between measured and computed SAR distributions are shown in Table II for different numbers of measurements k used for adaptation of antenna profiles and both phantoms. The computed SAR based on the adapted antenna profiles ($k>0$) is significantly more precise: In the homogeneous phantom, the error has been reduced by 30%, whereas in the heterogeneous phantom, the error reduction was even 50%.

Next, in Figs. 2–4 we show results based on antenna profile adaptations using arbitrary (but of course belonging to the same test series) control settings, while in Fig. 5 we present the closed-loop principle using sequentially optimized control settings as measurements become available (see Fig. 1).

Figure 2 shows a comparison between SAR distributions computed by original FDTD ($k=0$) and the corresponding MR measurement for a certain control setting u_a in the heterogeneous phantom. The deviation ΔSAR is as high as 4.7 W/kg. Figure 3 presents the improvement of the SAR prediction by use of only one adaptation step ($k=1$) in the heterogeneous phantom. Two predictions, one in Fig. 3(a) (for $k=0$, FDTD) and another in Fig. 3(b) (for $k=1$), are compared with the corresponding MR measurement shown in Fig. 3(c). The comparison in Fig. 3 is performed for control setting u_b. Left, in Fig. 3(a), the original FDTD predic-

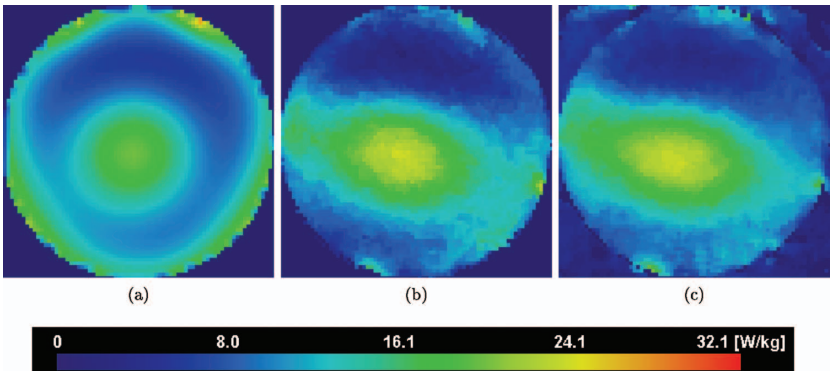

FIG. 4. Improvement of SAR prediction in the homogeneous phantom for the control setting u_d={Feet (21,26,34,14) Middle (24,9,7,327) Head (7,12,0,10)} by adaptation of antenna profiles based on only one measurement for a *different* control setting u_c={Feet(21,41,34,28) Middle (24,24,7,341) Head (7,27,0,24)}. (a) FDTD simulation for u_d:SAR(V_0,u_d), (b) improved SAR prediction SAR(V_1,u_d), and (c) associated measurement SAR^M(u_d). The deviation between (b) and (c) is reduced to ΔSAR=1.8 W/kg compared to the FDTD simulation (a) SAR(V_0,u_d) with ΔSAR=3.4 W/kg. Maximal measured SAR in the FOV: 24.3 W/kg, averaged measured SAR in FOV: 11.4 W/kg.

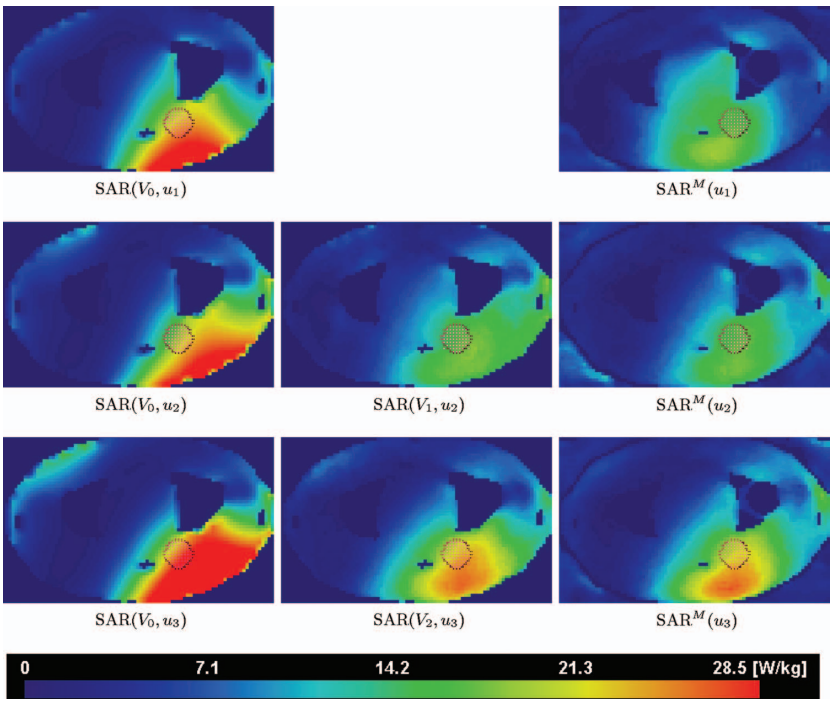

FIG. 5. Proof of concept for closed loop control based on adaptation of antenna profiles according to Fig. 1. **Left column:** FDTD without adaptation [SAR(V_0, u_i)]. **Middle column:** SAR computed using adapted antenna profiles [SAR(V_{i-1}, u_i)] with improved agreement with measurements. **Right column:** SAR measurement [SAR^M(u_i)] with improved SAR exposition of the target region (dotted circle). **Rows 1**, **2**, **3**: SAR distribution for control settings u_1, u_2 u_3 determined by successive maximization of SAR in the target region according to Fig. 1.

tion for u_b is shown. The deviation between Fig. 3(a) ($k=0$, FDTD) and measurement in Fig. 3(c) is as high as ΔSAR $=4.0$ W/kg. In Fig. 3(b) ($k=1$), the improved prediction for u_b is displayed, using the adapted antenna profiles based on the measurement for the *different* control setting, u_a, previously shown in Fig. 2. The deviation ΔSAR has been reduced from 4.0 to 2.6 W/kg. Note that the control setting u_a used for adaptation differs significantly in several channels from the compared setting u_b: In homogeneous medium, the difference between u_a and u_b would lead to a focus shift of about 10 cm.

In Fig. 4 a similar comparison as in Fig. 3 is carried out for control setting u_d, however for the homogeneous phantom. The deviation ΔSAR has been reduced from 3.4 to 1.8 W/kg. Again, a different setting u_c was used for adaptation. The difference between u_c and u_d leads to a focus shift of about 2–3 cm (measurement for u_c not shown).

Finally, Fig. 5 shows the application of the antenna profile adaptation to the closed loop control introduced in Fig. 1. In contrast to the situation in Figs. 3 and 4, the control settings have been obtained by simultaneous maximization of the SAR delivered to some target region and minimization of SAR outside this region (Table I, steps 6 and 7). Note that the quick convergence of the optimized control settings leads to small differences between the control settings used for adaptation and prediction, respectively, resulting in a better error reduction and simultaneously an improved heating of the target region.

IV. DISCUSSION

It has been shown that the adaptation of antenna profiles with a Gauss-Newton method based on few MR thermometry measurements can improve the prediction and the quality of SAR distributions significantly in several experimental settings. Error reductions of up to 50% compared to *a priori* simulations with the FDTD method have been observed. The most important effect of the improved accuracy is that therapy planning based on the adapted antenna profiles will lead to quite different optimal controls and deliver significantly more heat to the target region.

Given that the least squares approach is highly underdetermined ($6N=72$ degrees of freedom in the model to be fitted versus no more than five measurements) such that a complete identification of the model is impossible, this result is positively surprising. We suppose that the good initial model supplied by the FDTD simulation is of vital importance for the successful application of least-squares fitting.

Particularly remarkable is that most of the error reduction (70%–80%) is already achieved by adaptation based on the very first measurement. This fact can either be interpreted as an extraordinary success of the first adaptation step, or as a relative failure of subsequent adaptation steps. The first case would suggest the existence of an easily detectable, low-dimensional dominant error mode. In the second case, measurement errors such as noise or linearization error due to neglecting heat conduction, or possibly temperature-

dependent material parameters, are likely reasons for the limited progress achieved by subsequent adaptation steps. It is not yet clear which case applies.

A less pronounced but clearly visible outcome is that the error reduction is better in the heterogeneous phantom than in the homogeneous one. This can be attributed to the greater challenge that a complex heterogeneous geometry poses to an *a priori* simulation. On the other side, the measured SAR distribution in the heterogeneous phantom is more characteristic and pronounced (compare Fig. 3 and Fig. 4). In particular, positioning errors lead to larger deviations of the antenna profiles than in the homogeneous case—leaving more room for improvement by adaptation based on actual measurements.

The applicability of the adaptation to closed loop control has been demonstrated on phantoms, also under difficult conditions: adaptation on base of complementary control settings. Both the significant improvement already after one step and the better improvement in the heterogeneous phantom suggest that this approach is a first important step to online control of hyperthermia treatment of patients. For clinical applicability, additional problems have to be addressed, such as varying perfusion and patient movements. Control settings will be restricted to be therapeutically useful and cannot be expected to span the whole control space. Moreover, the cooling-down times are unacceptable in a treatment situation and have to be avoided by taking heat conduction into account when computing SAR from temperature measurements. Furthermore, the calculation of the initial value V_0 (e.g., FDTD) before the start of the actual therapy is not acceptable in clinical situation. The initial antenna profiles can be generated in a separate MR session and shift to the actual patient position at the beginning of the therapy.

ACKNOWLEDGMENTS

This work has been supported by grants of the Deutsche Forschungsgemeinschaft (DFG) (Project No. WU 235/1-2) and the Berliner Sparkassenstiftung Medizin (Project: "Oxygenation in Hyperthermia"). We gratefully appreciate the support.

[a]Electronic mail: mirko.weihrauch@charite.de Telephone: +4930 9417-1707; Fax: +4930 9417-1706

[1]J. van der Zee, D. G. González, G. C. van Rhoon, J. D. van Dijk, W. L. van Putten, and A. A. Hart, "Comparison of radiotherapy alone with radiotherapy plus hyperthermia in locally advanced pelvic tumours: a prospective, randomised, multicentre trial. Dutch Deep Hyperthermia Group," Lancet **355**(9210), 1119–1125 (2000).

[2]G. Sreenivasa, B. Hildebrandt, S. Kümmel, K. Jungnickel, C. H. Cho, W. Tilly, D. Böhmer, V. Budach, R. Felix, and P. Wust, "Radiochemotherapy combined with regional pelvic hyperthermia induces high response and resectability rates in patients with nonresectable cervical cancer," Int. J. Radiat. Oncol., Biol., Phys. **66**(4), 1159–1167 (2006).

[3]R. D. Issels, L. H. Lindner, P. Wust, P. Hohenberger, K. Jauch, S. Daugaard, U. Mansmann, W. Hiddemann, J. Blay, and J. Verweij, "Regional hyperthermia (RHT) improves response and survival when combined with systemic chemotherapy in the management of locally advanced, high grade soft tissue sarcomas (STS) of the extremities, the body wall and the abdomen: a phase III randomised prospective trial (EORTC-ESHO intergroup trial)," in *ASCO*, 2007.

[4]B. Rau, P. Wust, W. Tilly, J. Gellermann, C. Harder, H. Riess, V. Budach, R. Felix, and P. M. Schlag, "Preoperative radiochemotherapy in locally advanced or recurrent rectal cancer: regional radiofrequency hyperthermia correlates with clinical parameters," Int. J. Radiat. Oncol., Biol., Phys. **48**(2), 381–391 (2000).

[5]J. Gellermann, B. Hildebrandt, R. Issels, H. Ganter, W. Wlodarczyk, V. Budach, R. Felix, P.-U. Tunn, P. Reichardt, and P. Wust, "Noninvasive magnetic resonance thermography of soft tissue sarcomas during regional hyperthermia: correlation with response and direct thermometry," Cancer **107**(6), 1373–1382 (2006).

[6]P. Wust, C. H. Cho, B. Hildebrandt, and J. Gellermann, "Thermal monitoring: invasive, minimal-invasive and non-invasive approaches," Int. J. Hyperthermia **22**(3), 255–262 (2006).

[7]P. Wust, M. Seebass, J. Nadobny, P. Deuflhard, G. Mönich, and R. Felix, "Simulation studies promote technological development of radiofrequency phased array hyperthermia," Int. J. Hyperthermia **12**(4), 477–494 (1996).

[8]K. D. Paulsen, S. Geimer, J. Tang, and W. E. Boyse, "Optimization of pelvic heating rate distributions with electromagnetic phased arrays," Int. J. Hyperthermia **15**(3), 157–186 (1999).

[9]H. Kroeze, J. B. V. de Kamer, A. A. D. Leeuw, and J. J. Lagendijk, "Regional hyperthermia applicator design using FDTD modelling," Phys. Med. Biol. **46**(7), 1919–1935 (2001).

[10]M. Seebass, R. Beck, J. Gellermann, J. Nadobny, and P. Wust, "Electromagnetic phased arrays for regional hyperthermia: optimal frequency and antenna arrangement," Int. J. Hyperthermia **17**(4), 321–336 (2001).

[11]K. S. Yee, "Numerical solution of initial boundary value problems involving Maxwell's equations in isotropic media," IEEE Trans. Antennas Propag. **17**, 585–589 (1966).

[12]D. M. Sullivan, O. P. Gandhi, and A. Taflove, "Use of the finite-difference time-domain method for calculating EM absorption in man models," IEEE Trans. Biomed. Eng. **35**(3), 179–186 (1988).

[13]A. Taflove, *Computational Electrodynamics. The Finite-Difference Time-Domain Method* (Artech House, Boston, London, 1995).

[14]R. Beck, P. Deuflhard, R. Hiptmair, R. H. W. Hoppe, and B. Wohlmuth, "Adaptive multilevel methods for edge element discretizations of Maxwell's equations," Surv. Math. Ind. **8**, 271–312 (1999).

[15]H. H. Pennes, "Analysis of tissue and arterial blood temperatures in the resting human forearm. 1948," J. Appl. Physiol. **85**(1), 5–34 (1998).

[16]B. J. James and D. M. Sullivan, "Direct use of CT scans for hyperthermia treatment planning," IEEE Trans. Biomed. Eng. **39**(8), 845–851 (1992).

[17]J. B. V. de Kamer, H. Kroeze, A. A. D. Leeuw, and J. J. Lagendijk, "Quasistatic zooming of FDTD E-field computations: the impact of down-scaling techniques," Phys. Med. Biol. **46**(5), 1539–1551 (2001).

[18]J. Nadobny, H. Fähling, M. J. Hagmann, P. F. Turner, W. Wlodarczyk, J. M. Gellermann, P. Deuflhard, and P. Wust, "Experimental and numerical investigation of feed-point parameters in a 3-D hyperthermia applicator using different FDTD models of feed networks," IEEE Trans. Biomed. Eng. **49**(11), 1348–1359 (2002).

[19]J. Gellermann, W. Wlodarczyk, H. Ganter, J. Nadobny, H. Fähling, M. Seebass, R. Felix, and P. Wust, "A practical approach to thermography in a hyperthermia/magnetic resonance hybrid system: validation in a heterogeneous phantom," Int. J. Radiat. Oncol., Biol., Phys. **61**(1), 267–277 (2005).

[20]J. Nadobny, W. Wlodarczyk, L. Westhoff, J. Gellermann, R. Felix, and P. Wust, "A clinical water-coated antenna applicator for MR-controlled deep-body hyperthermia: a comparison of calculated and measured 3-D temperature data sets," IEEE Trans. Biomed. Eng. **52**(3), 505–519 (2005).

[21]J. Gellermann, M. Weihrauch, C. H. Cho, W. Wlodarczyk, H. Fähling, R. Felix, V. Budach, M. Weiser, J. Nadobny, and P. Wust, "Comparison of MR-thermography and planning calculations in phantoms," Med. Phys. **33**(10), 3912–3920 (2006).

[22]J. Lunze, *Regelungstechnik Band 2—Mehrgrößensysteme, digitale Regelung.*, 2nd ed. (Springer Verlag, Berlin, 2001).

[23]J. Lunze, *Regelungstechnik Band 1—Systemtheoretische Grundlagen, Analyse und Entwurf einschleifiger Regelungen.*, 3rd ed. (Springer Verlag, Berlin, 2001).

[24]E. Hutchinson, M. Dahleh, and K. Hynynen, "The feasibility of MRI feedback control for intracavitary phased array hyperthermia treatments," Int. J. Hyperthermia **14**(1), 39–56 (1998).

[25]D. Arora, M. Skliar, and R. B. Roemer, "Model-predictive control of hyperthermia treatments," IEEE Trans. Biomed. Eng. **49**(7), 629–639 (2002).

[26]P. Wust, J. Gellermann, M. Seebass, H. Fähling, W. Wlodarczyk, J. Nadobny, B. Rau, B. Hildebrandt, A. Oppelt, and R. Felix, "Teilkörperhyperthermie mit einem Radiofrequenz-Multiantennen-Applikator unter online Kontrolle in einem 1,5 T MR-Tomographen," Fortschr. Röntgenstr. **176**, 363–374 (2004).
[27]J. Gellermann, W. Wlodarczyk, A. Feussner, H. Fähling, J. Nadobny, B. Hildebrandt, R. Felix, and P. Wust, "Methods and potentials of magnetic resonance imaging for monitoring radiofrequency hyperthermia in a hybrid system," Int. J. Hyperthermia **21**(6), 497–513 (2005).
[28]M. E. Kowalski, B. Behnia, A. G. Webb, and J.-M. Jin, "Optimization of electromagnetic phased-arrays for hyperthermia via magnetic resonance temperature estimation," IEEE Trans. Biomed. Eng. **49**(11), 1229–1241 (2002).
[29]M. E. Kowalski and J. M. Jin, "A temperature-based feedback control system for electromagnetic phased-array hyperthermia: theory and simulation," Phys. Med. Biol. **48**(5), 633–651 (2003).
[30]S. K. Das, E. A. Jones, and T. V. Samulski, "A method of MRI-based thermal modelling for a RF phased array," Int. J. Hyperthermia **17**(6), 465–482 (2001).
[31]T. Köhler, P. Maass, P. Wust, and M. Seebass, "A fast algorithm to find optimal controls of multiantenna applicators in regional hyperthermia," Phys. Med. Biol. **46**(9), 2503–2514 (2001).
[32]P. Wust, H. Stahl, J. Löffel, M. Seebass, H. Riess, and R. Felix, "Clinical, physiological and anatomical determinants for radiofrequency hyperthermia," Int. J. Hyperthermia **11**(2), 151–167 (1995).
[33]W. Tilly, P. Wust, B. Rau, C. Harder, J. Gellermann, P. Schlag, V. Budach, and R. Felix, "Temperature data and specific absorption rates in pelvic tumours: predictive factors and correlations," Int. J. Hyperthermia **17**(2), 172–188 (2001).
[34]P. Deuflhard and A. Hohmann, *Numerische Mathematik I.*, 3rd ed. (Walter de Gruyter, Berlin, 2002).
[35]P. Wust, R. Beck, J. Berger, H. Fähling, M. Seebass, W. Wlodarczyk, W. Hoffmann, and J. Nadobny, "Electric field distributions in a phased-array applicator with 12 channels: measurements and numerical simulations," Med. Phys. **27**(11), 2565–2579 (2000).
[36]P. Wust, H. Fähling, W. Wlodarczyk, M. Seebass, J. Gellermann, P. Deuflhard, and J. Nadobny, "Antenna arrays in the SIGMA-eye applicator: interactions and transforming networks," Med. Phys. **28**(8), 1793–1805 (2001).
[37]J. Gellermann, W. Wlodarczyk, B. Hildebrandt, H. Ganter, A. Nicolau, B. Rau, W. Tilly, H. Fähling, J. Nadobny, R. Felix, and P. Wust, "Noninvasive magnetic resonance thermography of recurrent rectal carcinoma in a 1.5 Tesla hybrid system," Cancer Res. **65**(13), 5872–5880 (2005).
[38]J. D. Poorter, C. D. Wagter, Y. D. Deene, C. Thomsen, F. Ståhlberg, and E. Achten, "Noninvasive MRI thermometry with the proton resonance frequency (PRF) method: in vivo results in human muscle," Magn. Reson. Med. **33**(1), 74–81 (1995).
[39]D. Stalling, M. Westerhoff, and H.-C. Hege, "Amira: a highly interactive system for visual data analysis," in *The Visualization Handbook*, edited by C. D. Hansen and C. R. Johnson (Elsevier, Amsterdam, 2005), Chap. 38, pp. 749–767.
[40]G. Sreenivasa, J. Gellermann, B. Rau, J. Nadobny, P. Schlag, P. Deuflhard, R. Felix, and P. Wust, "Clinical use of the hyperthermia treatment planning system HyperPlan to predict effectiveness and toxicity," Int. J. Radiat. Oncol., Biol., Phys. **55**(2), 407–419 (2003).
[41]J. Nadobny, D. Sullivan, P. Wust, M. Seebass, P. Deuflhard, and R. Felix, "A high-resolution interpolation at arbitrary interfaces for the FDTD method," IEEE Trans. Microwave Theory Tech. **46**(11), 1759–1766 (1998).

Selbständigkeitserklärung

„Ich, Mirko Weihrauch, erkläre, dass ich die vorgelegte Dissertationsschrift mit dem Thema: *Regelschleife für die Magnetresonanz-kontrollierte Teilkörper-Hyperthermie*, selbst verfasst und keine anderen als die angegebenen Quellen und Hilfsmittel benutzt, ohne die (unzulässige) Hilfe Dritter verfasst und auch in Teilen keine Kopien anderer Arbeiten dargestellt habe“

(Mirko Weihrauch) 21. Juli 2008

Der Promovend hatte folgenden Anteil an den vorgelegten Publikationen:

Publikation 1: Gellermann J., M. Weihrauch, C. H. Cho, W. Wlodarczyk, H. Fähling, R. Felix, V. Budach, M. Weiser, J. Nadobny und P. Wust: *Comparison of MR-thermography and planning calculations in phantoms.* Med. Phys., 33(10):3912–3920, Oct 2006.

45 Prozent

Beitrag im Einzelnen: Planung und Durchführung der Messreihen in Zusammenarbeit mit Dr. Gellermann, Entwicklung und Implementierung der Software zur statistischen Auswertung der Messreihen, Visualisierung der Ergebnisse, Aufarbeitung der Ergebnisse, Vorformulierung der Arbeit, Ausarbeitung der endgültigen Formulierung und der Reviews in Zusammenarbeit mit Prof. Wust, Dr. Nadobny, Dr. Weiser und Dr. Gellermann.

Publikation 2: Gellermann J., J. Göke, R. Figiel, M. Weihrauch, C. H. Cho, V. Budach, R. Felix und P. Wust: *Simulation of different applicator positions for treatment of a presacral tumour.* Int J Hyperthermia, 23(1):37–47, Feb 2007.

35 Prozent

Beitrag im Einzelnen: Mitarbeit bei der statistischen Aufarbeitung der Messreihen, Mitarbeit bei der Formulierung der Arbeit und bei den Reviews.

Publikation 3: Weihrauch M., P. Wust, M. Weiser, J. Nadobny, S. Eisenhardt, V. Budach und J. Gellermann: *Adaptation of antenna profiles for control of MR guided hyperthermia (HT) in a hybrid MR-HT system.* Med. Phys., 34(12):4717–4725, Dec 2007.

90 Prozent

Beitrag im Einzelnen: Konzeption der Arbeit zusammen mit Prof. Wust, Planung und Durchführung der Messreihen, Entwicklung und Implementierung der Software zur Vorverarbeitung der Thermometriedaten, Entwicklung und Implementierung der Software zur statistischen Auswertung der Messreihen, Entwicklung der Algorithmen zur Adaptation der Antennenprofile in Kooperation mit Dr. Weiser, Implementierung und Anwendung der Software zur Adaptation der Antennenprofile, Aufarbeitung der Ergebnisse und Formulierung der Arbeit, Formulierung der endgültigen Fassung in Zusammenarbeit mit Prof. Wust, Dr. Nadobny, Dr. Weiser und Dr. Gellermann. Nachbearbeitung der Reviews.

Danksagung

Bei Herrn Prof. Dr. V. Budach sowie dem früheren Leiter der Abteilung Prof. Dr. Dr. h. c. R. Felix möchte ich mich für die Möglichkeit, diese Arbeit am Hybridsystem der Charité durchführen zu können, sehr bedanken.

Besonderer Dank geht an meine Betreuer Herrn Prof. Dr. P. Wust und Frau Dr. J. Gellermann. Ihr jahrelanger unermüdlicher Einsatz für die Hyperthermie und ihre Vorarbeiten haben das Projekt erst realisierbar gemacht. Sie standen immer als Ansprechpartner zur Verfügung und haben mit vielen Ratschlägen und Ihrem fundierten Wissen zur Fertigstellung dieser Arbeit entscheidend beigetragen. Meinem Betreuer Herrn Dr. M. Weiser vom Konrad-Zuse-Zentrum für Informationstechnik Berlin bin ich ebenfalls besonders dankbar. Neben der Formulierung der Algorithmen stand er als Ansprechpartner bei mathematischen Fragestellungen immer zur Verfügung.

Bei Herrn Dr. J. Nadobny möchte ich mich für die zeitintensive Unterstützung bei der Formulierung der Publikationen sowie die Diskussionen der Hyperthermieplanungsrechnungen bedanken. Herrn Dr. W. Wlodarczyk möchte ich danken für die Beantwortung vieler Fragen im Rahmen der MR-Thermometrie. Herrn Fähling sei an dieser Stelle der Dank für die Optimierung und die ständige Wartung des Hyperthermieapplikators sowie die Diskussion über die Antennenprofile ausgesprochen. Frau C.-H. Cho, Frau H. Ganter und Frau M. Weis-Mehling bin ich für so manche Zuarbeit dankbar.

Bei Herrn Dipl.-Biophys. S. Eisenhardt, Herrn R. Figiel und Herrn J. Göke möchte ich mich für diverse Zuarbeiten (MR-Thermometrie, Positionskorrektur der Antennenprofile, etc.) sehr bedanken. Für die gute Zusammenarbeit möchte ich mich bei Herrn Dr. L. Lüdemann, Herrn Dipl.-Inf. H. Rehbein, Hernn Dipl.-Phys. J.-T. Ollek und Herrn T. Mensing bedanken.

Ein Dankeschön geht auch an Herrn Dr. M. Seebaß und Herrn Dr. D. Stalling von der Firma Visage Imaging GmbH und Herrn Dr. L. Lüdemann, die bei Fragen zur Planungssoftware AmiraHyperplan oft weiterhelfen konnten.

Frau S. Jentsch danke ich für die Unterstützung bei der Durchführung der Experimente und Frau Dipl.-Reha. Päd. C. Bürgel für das Korrekturlesen.

Der Firma BSD Medical Corporation und der Firma Dr. Sennewald Medizintechnik GmbH danke ich für die Implementierung der Schnittstelle zum Hyperthermiesystem, die eine wesentliche Erleichterung bei den Erwärmungsexperimenten und im alltäglichen Betrieb gewährleistet.

Schließlich möchte ich mich bei der Deutschen Forschungsgemeinschaft und der Berliner Sparkassenstiftung Medizin für die Förderung meines Forschungsprojekts sehr bedanken.

Lebenslauf

„Mein Lebenslauf wird aus datenschutzrechtlichen Gründen in der elektronischen Version meiner Arbeit nicht veröffentlicht.“